How space-time modulations modify spoof surface plasmons and scattering properties in acoustic metagratings

Kim Pham
IMSIA, CNRS, EDF, CEA, ENSTA Paris, Institut Polytechnique de Paris, 828 Bd des Maréchaux, 91732 Palaiseau, France

Agnès Maurel
Institut Langevin, ESPCI Paris, Université PSL, CNRS, 1 rue Jussieu, 75005 Paris, France

(Received 31 January 2023; revised 15 May 2023; accepted 27 June 2023; published 7 July 2023)

We analyze the propagation of acoustic waves in a space-time (ST) modulated grating moving at constant velocity and surrounded by air. By means of asymptotic techniques, we derive in the subwavelength regime a homogenized nonreciprocal model in which the grating is replaced by an equivalent bianisotropic slab at the boundaries of which effective jump conditions apply, that encapsulate the effect of the evanescent fields. This effective framework allows to characterize analytically the properties of ST modulated metagratings in terms of scattering properties and guided wave dispersion. First we derive the closed-form dispersion relation of spoof surface plasmon polaritons (SPPs) and show the appearance of multiple redshifted or blueshifted branches due to the ST modulation. Next, we provide in the radiative region closed-form expressions for the Brewster angle and Fabry-Pérot resonances and show how the ST modulation heavily modifies the complex spectra. Finally, we illustrate the potential of such a system to achieve negative refraction or perfect transparency by playing on the modulation. Throughout the study, our analysis is validated by comparison with direct numerical simulations.

DOI: 10.1103/PhysRevB.108.024303

I. INTRODUCTION

After seminal works [1,2], wave propagation in materials with space and time dependencies has been studied in the 2000s in an almost exhaustive way by Lurie [3–8] who introduced the terms of dynamic materials being either kinematic with time-independent material properties in a moving material or activated with time-dependent material properties in a material at rest. In recent years there has been a growing interest in these latter materials, renamed space-time modulated materials as they produce nonreciprocal propagation [9–14], frequency conversions through the appearance of space-time diffraction orders [15–18], and many systems have been proposed and experimentally realized for practical applications [10,13,16,17,19,20]. Among the exceptional properties of these media, the nonreciprocal propagation that occurs even in the low-frequency regime is the rule due to the properties shared with the media supporting a flow [21]. It is manifested by enriched relations between the fields, with the appearance of a coupling parameter, called magnetoelectric coupling in electromagnetism [22] or Willis coupling in elastodynamics and acoustics [9,23]. It is interesting to note that such nonreciprocal materials, without recourse to any modulations, are the perfect electromagnetic conductors (PEMC) introduced in [24,25] as a generalization of perfect electrical conductors and perfect magnetic conductors (these limiting cases with parameters tending to 0 and others tending to infinity are reciprocal). The case of perfect conductors has an acoustic analog which are rigid materials; in this context, infinitely anisotropic dispersion in plate arrays has been used to control the dispersion of surface waves [26], to obtain broadband transmission at the Brewster angle [27–29] and to produce negative refraction [29].

From a theoretical point of view, the description of modulated media at the microscopic scale using the notion of effective medium is now classical. It has been extended to space-time modulated media in [3,4,30,31] and more recently in [9,32–34] with a particular emphasis on bianisotropy and its implications. We study here an acoustic metagrating whose rigid parts are modulated in time and space (Fig. 1) and to set the scene, our goal is to understand and capture precisely the influence of temporal modulations on the dispersion of guided waves of the spoof surface plasmon (SPPs) type and on scattering spectra in the radiative region as shown in Fig. 2. To do this, we propose a homogenization approach which includes the effects of the finite size of the grating, that is to say, the effect of the evanescent field triggered at the interfaces of the grating with the surrounding air. To validate our model, we rely on numerical simulations based on multimodal analysis recently proposed in [35].

The paper is organized as follows. In Sec. II, we give the form of the homogenized model whose derivation is detailed in the Appendix B; the homogenization in the bulk is classical and it is based on the previously mentioned work, the homogenization at the grating interfaces is more involved and we extend a previous study performed for a grating without time modulation [36]. In Sec. III, the effective dispersion is obtained and discussed and we give the general effective solution of the scattering problem for finite-size gratings. This solution allows us to analyze the characteristics of guided waves supported by the grating; this is done in Sec. IV. We show that these modulated SPPs have a propagation

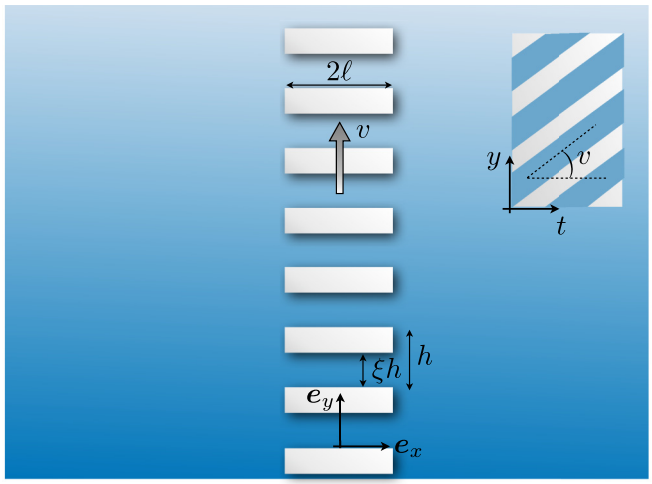

FIG. 1. Space-time modulated acoustic grating of extended 2ℓ made of a h-periodic lamination alternating air and rigid parts modulated in time at constant speed v in direction $\boldsymbol{e}_y$.

which can be blueshifted or redshifted, as observed for time-modulated device [37], and that the number of their branches with increasing modulation velocity is only limited by the appearance of a new diffraction order. In Sec. V, we discuss the scattering properties in the radiative region; we focus in particular on the conditions for perfect transmission which result from an interaction between the dispersive propagation in the grating and the boundary layer effects. This is further used to analyze positive and negative refractions in modulated gratings that share common features with refraction in unmodulated gratings of tilted plates [28,29].

II. HOMOGENIZED MODEL FOR A METAGRATING OF FINITE SIZE

In this section, we first formulate the direct problem whose semianalytical solution based on multimodal analysis was recently proposed in [35] and which will serve as a reference solution throughout our study. We then give the form of the homogenized problem whose derivation based on asymptotic analysis is detailed in Appendix B.

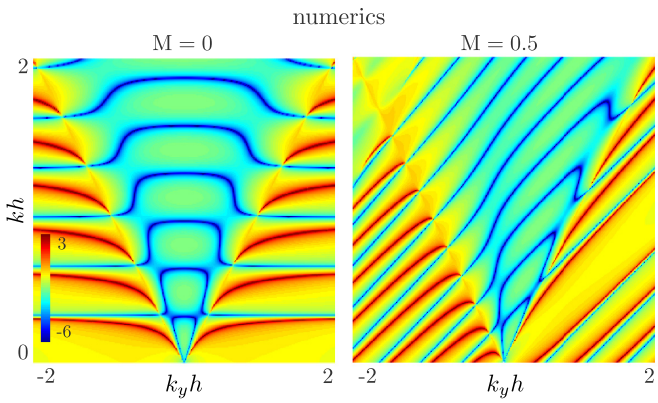

FIG. 2. Reflection spectra in the (k, k_y) space for an unmodulated metagrating at normalized modulation velocity $\mathrm{M} = v/c = 0$ and a space-time modulated metagrating at $\mathrm{M} = v/c = 0.5$ ($2\ell = 10h$, $\xi = 0.8$).

A. Actual problem

In the air, the acoustic waves are governed by the linearized Euler equations

$$\rho \frac{\partial \boldsymbol{u}}{\partial t} = -\nabla p, \quad \mathrm{div}\boldsymbol{u} + \frac{1}{\rho c^2}\frac{\partial p}{\partial t} = 0, \tag{1}$$

with $\boldsymbol{u}$ the velocity, p the acoustic pressure, ρ the mass density, and c the speed of sound. Following [4], we introduce the velocity potential φ so that the first equation (1) is written as

$$\begin{pmatrix} \boldsymbol{u} \\ \frac{p}{Z} \end{pmatrix} = \begin{pmatrix} \mathsf{I} & 0 \\ 0 & 1 \end{pmatrix} \begin{pmatrix} \nabla\varphi \\ -\frac{1}{c}\frac{\partial\varphi}{\partial t} \end{pmatrix}, \tag{2}$$

with I the identity matrix 2×2 ($Z = \rho c$ is the impedance) while the conservation of mass remains the same, namely,

$$\mathrm{div}\boldsymbol{u} + \frac{1}{Zc}\frac{\partial p}{\partial t} = 0. \tag{3}$$

We obtain for φ the equation of propagation

$$\frac{\partial^2\varphi}{\partial x^2} + \frac{\partial^2\varphi}{\partial y^2} - \frac{1}{c^2}\frac{\partial^2\varphi}{\partial t^2} = 0. \tag{4}$$

Eventually, (2) and (3) are complemented by Robin-type condition on the space-time modulated rigid boundaries,

$$Z\boldsymbol{u}\cdot\boldsymbol{n} = \mathrm{M}(\boldsymbol{e}_y\cdot\boldsymbol{n})\, p, \tag{5}$$

where $\mathrm{M} = v/c$, with $\boldsymbol{v} = v\boldsymbol{e}_y$ the *constant* velocity of the modulation (see Fig. 1). This boundary condition results from the conservation of mass in the presence of an external process [8] that modulates the material properties of the medium along the moving boundaries (see Appendix A for a detailed analysis).

B. Homogenized problem

After homogenization, the calculation of which is detailed in Appendix B, we obtain an effective model containing two ingredients. In the space-time modulated grating, the effective, homogeneous, medium is governed by the mass conservation (3) and a homogeneous anisotropic constitutive relation given by

$$\begin{pmatrix} \boldsymbol{u} \\ \frac{p}{Z} \end{pmatrix} = \xi \begin{pmatrix} 1 & 0 & 0 \\ 0 & -\frac{\mathrm{M}^2}{1-\mathrm{M}^2} & \frac{\mathrm{M}}{1-\mathrm{M}^2} \\ 0 & -\frac{\mathrm{M}}{1-\mathrm{M}^2} & \frac{1}{1-\mathrm{M}^2} \end{pmatrix} \begin{pmatrix} \nabla\varphi \\ -\frac{1}{c}\frac{\partial\varphi}{\partial t} \end{pmatrix}, \tag{6}$$

which gives us the following effective equation of propagation:

$$\frac{\partial^2\varphi}{\partial x^2} - \frac{1}{1-\mathrm{M}^2}\left(\mathrm{M}\frac{\partial}{\partial y} + \frac{1}{c}\frac{\partial}{\partial t}\right)^2\varphi = 0. \tag{7}$$

These equations are completed by jump conditions at the extremities of the grating $x_\mathrm{e} = \pm\ell$ of the form

$$\begin{aligned} [\![\varphi]\!] &= \frac{h\mathcal{B}}{\sqrt{1-\mathrm{M}^2}}\,\overline{u_x}, \\ [\![u_x]\!] &= \frac{-h\mathcal{C}}{(1-\mathrm{M}^2)^{3/2}}\left(\frac{\partial}{\partial y} + \frac{\mathrm{M}}{c}\frac{\partial}{\partial t}\right)^2\overline{\varphi}, \end{aligned} \tag{8}$$

where we have defined the jump and the mean value of the fields $A = \{\varphi, u_x\}$ as follows: $[\![A]\!] = A^+ - A^-$ and $\overline{A} = 1/2(A^+ + A^-)$, with $A^\pm = A(x_e^\pm, y, t)$ the values of A on both sides of the interface at $x = x_e$. The coefficients $(\mathcal{B}, \mathcal{C})$ are real, dimensionless, parameters that depend only on ξ, with

$$\mathcal{B} = -\frac{1}{\pi}\log\left(\sin\frac{\pi\xi}{2}\right), \quad \mathcal{C} \simeq \frac{\pi\xi^2}{16}. \tag{9}$$

The jump conditions (8) which involve the grating periodicity h tell us that the grating does not behave as a homogeneous slab; these conditions encode the effect of the boundary layers, that is to say, the effect of the evanescent fields triggered at the grating boundaries. We notice that for $\mathrm{M} = 0$, (6)–(8) correspond to the homogenized model of a rigid, fixed, grating studied in [36,38]. For $\mathrm{M} \neq 0$, it is visible that the time-reversal invariance $t \to -t$, as well as the reciprocity in the scattering process $(x, y) \to -(x, y)$, are broken [14] and they are restored if one imposes in addition a modulation switch $\mathrm{M} \to -\mathrm{M}$ as it has been reported for acoustic propagation in the presence of a flow [39]. Next, the grating that supports propagation along the x axis has mirror symmetry, i.e., it leaves the problem invariant under the transformation $(x, y) \to (-x, y)$. This is different from the case of tilted rigid plates at $\mathrm{M} = 0$ as in [29], where the system is nonsymmetric and of course reciprocal.

III. PROPERTIES OF THE EFFECTIVE MODEL

From now on, we consider the harmonic regime with a time dependence $e^{-i\omega t}$ (ω is the frequency). Denoting $k = \omega/c$ the wave number in the air, the effective model holds for a single mode that we call mode 0, that is to say, below the thresholds for the appearance of higher propagating modes (or higher diffraction orders). Denoting k_y the component of the wave vector along y, this mode 0 is propagating in the radiative region that is to say above the radiative line when $k > k_y$ and it is evanescent below when $k < k_y$. In the numerics, the thresholds for the appearance of higher propagating modes (or higher diffraction orders), labeled by n, are given by

$$k_n^2 = \left(k + \mathrm{M}\frac{2n\pi}{h}\right)^2 > \left(k_y + \frac{2n\pi}{h}\right)^2, \quad n \text{ integer} \tag{10}$$

and the mode n is associated with frequency $\omega_n = ck_n$ [35]. It results that higher modes ($|n| > 0$) can become propagating in the radiative region of the mode 0 which is expected, but also in the nonradiative region of the mode 0 which is specific to modulated gratings.

A. Dispersion relation in the effective grating

By noting $\mathbf{K} = (K_x, K_y)$ the effective wave vector, the dispersion relation is deduced from (7) and it is written

$$K_x\cos\alpha \pm K_y\sin\alpha = \pm k \quad (\Delta^\pm), \tag{11}$$

with

$$\cos\alpha = \sqrt{1-\mathrm{M}^2}, \quad \sin\alpha = \mathrm{M}, \tag{12}$$

and $\alpha \in (-\pi/2, \pi/2)$. It corresponds to two, mirror-symmetric, lines $\Delta^\pm$ of slope $\pm\alpha$ with respect to the axis of K_y (Fig. 3). For $\mathrm{M} = 0$, these two lines are vertical, with

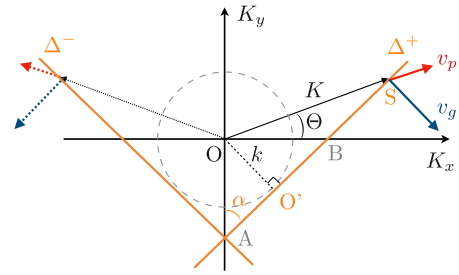

FIG. 3. Dispersion relation (11) formed by two straight lines $\Delta^\pm$ tangent to the circle of radius k and of angles $\pm\alpha$ with respect to the axis K_y (here, $\alpha < 0$).

$K_x = \pm k$ whatever the value of K_y, which corresponds to the one-dimensional propagation along the rigid plates as expected [36].

We now calculate the phase and group velocities $\boldsymbol{v}_p$ and $\boldsymbol{v}_g$. We define $K_x = K\cos\Theta$, $K_y = K\sin\Theta$ as well as the geometrical parameter $\delta = \mathrm{O'S}/k$ with S the extremity of the wave vector $\mathbf{K}$ [and $\mathrm{O'S} = K\sin(\Theta - \alpha)$, Fig. 3]. We obtain $K = k\sqrt{1+\delta^2}$ and

$$\boldsymbol{v}_p = \frac{c}{\sqrt{1+\delta^2}}\begin{pmatrix}\cos\Theta\\ \sin\Theta\end{pmatrix}, \quad \boldsymbol{v}_g = c\begin{pmatrix}\cos\alpha\\ \sin\alpha\end{pmatrix}. \tag{13}$$

The direction $\Theta = \alpha$ is particular since we have then $\delta = 0$, hence, $K = k$ and $v_p = v_g = c$, that is to say, the grating behaves as free air.

B. Solution of the homogenized problem for a grating of finite extent

As is the rule, the homogenization process has made spatial lamination disappear. The resulting problem for a finite-size grating is hence translational invariant, and explicit solutions are therefore available. For an incident wave with wave number k_y, it reads as

$$\varphi = e^{ik_y y}\begin{cases} e^{ik_x(x+\ell)} + re^{-ik_x(x+\ell)}, & x \in (-\infty, -\ell)\\ A_\mathrm{s}\cos K_x x + A_\mathrm{a}\sin K_x x, & x \in (-\ell, \ell)\\ te^{ik_x(x-\ell)}, & x \in (\ell, +\infty).\end{cases} \tag{14}$$

The component k_y is conserved and, from the preceding section, the condition $k_y = K_y$ is always possible (see Fig. 3). For $|x| > \ell$, φ satisfies (4), and for $|x| < \ell$, φ satisfies (7), hence,

$$k_x^2 = k^2 - k_y^2, \quad K_x^2 = \frac{(k - \mathrm{M}k_y)^2}{1-\mathrm{M}^2}. \tag{15}$$

By using (8) in (14), we obtain four relations for the four unknowns (r, t, a^-, a^+), leading to

$$t = \frac{1}{2}\left(\frac{Z_a}{Z_a^*} - \frac{Z_s}{Z_s^*}\right), \quad r = -\frac{1}{2}\left(\frac{Z_s}{Z_s^*} + \frac{Z_a}{Z_a^*}\right), \tag{16}$$

with

$$Z_s = \xi K_x\tan K_x\ell(1 + ik_x\mathcal{B}_\mathrm{M}) - (ik_x + \mathcal{C}_\mathrm{M}),$$
$$Z_a = \xi K_x(1 + ik_x\mathcal{B}_\mathrm{M}) + (ik_x + \mathcal{C}_\mathrm{M})\tan K_x\ell,$$

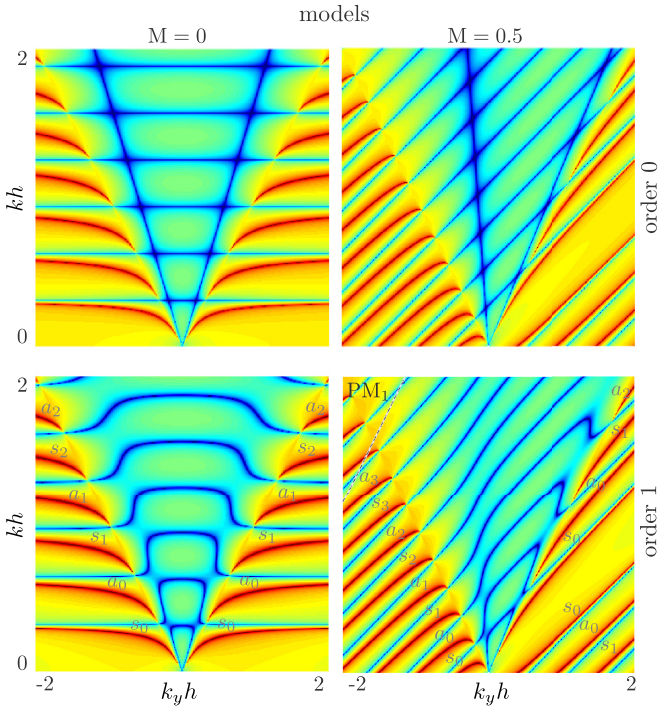

FIG. 4. Reflection spectra given by the homogenized model at the order 1 from (16) and (17) and for comparison, at the dominant order 0 [by setting $\mathcal{B} = \mathcal{C} = 0$ in (17)]. Same representation as in Fig. 2.

where we have defined

$$\mathcal{B}_{\mathrm{M}} = \frac{h\mathcal{B}}{\sqrt{1-\mathrm{M}^2}}, \quad \mathcal{C}_{\mathrm{M}} = \frac{h\mathcal{C}(k_y - \mathrm{M}k)^2}{(1-\mathrm{M}^2)^{3/2}}. \tag{17}$$

The predictive force of our model is illustrated in Figs. 4 and 5 where we use the grating geometry for which the spectra in Fig. 2 were obtained numerically. For M = 0 and 0.5, we plot the reflection spectra given by the full effective model (at order 1), i.e., r in (16) and (17) and, for comparison, those given by the model at leading order (order 0) obtained by setting $\mathcal{B} = \mathcal{C} = 0$ in (17). It can be seen that the order-0 model already gives a satisfactory picture of the acoustic response of the modulated grating although noticeable discrepancies are visible in the radiative region ($k > |k_y|$). The model at order 1, by taking into account the effects of the evanescent field at the boundaries of the modulated grating, improves the prediction which becomes almost indistinguishable from the

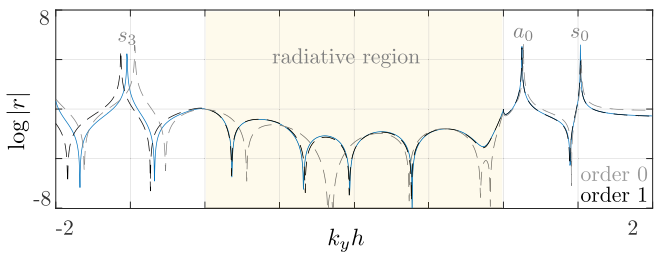

FIG. 5. Profiles from Fig. 4 for $kh = 1$; direct numerics (plain blue line), model at the order 0 (dashed gray line) and at the order 1 (dashed black line).

numerical solution. This is valid except above the threshold for the appearance of the propagating mode 1 (region denoted PM_1) when $(k - k_y)h > 2\pi(1 - \mathrm{M})$, from (10). We notice that part of this PM_1 region lies below the radiative line for $-k_y > k > 0$ which means that mode 1 can be propagating while mode 0 is evanescent.

In the following sections, we analyze in detail the acoustic response of the modulated gratings outside and inside the radiative region. We can anticipate from our observations in Figs. 4 and 5 that the analysis outside the radiative region will be facilitated because the simplified model at order 0 is already very satisfactory; this is not the case anymore in the radiative region.

IV. SPACE-TIME MODULATED SPOOF SURFACE PLASMONS

A. Redshifted and blueshifted SPPs

Guided waves are solutions to the effective problem (7) and (8) in absence of source; due to mirror symmetry, we get symmetric SPPs, termed s-SPPs [$\varphi(-x, y) = \varphi(x, y)$]

$$\varphi(x, y) = e^{ik_y y}\begin{cases} A_{\mathrm{s}} \cos K_x x, & x \in (0, \ell) \\ t_{\mathrm{s}} e^{-\sigma(x-\ell)}, & x \in (\ell, +\infty) \end{cases} \tag{18}$$

and antisymmetric a-SPPs [$\varphi(-x, y) = -\varphi(x, y)$]

$$\varphi(x, y) = e^{ik_y y}\begin{cases} A_{\mathrm{a}} \sin K_x x, & x \in (0, \ell), \\ t_{\mathrm{a}} e^{-\sigma(x-\ell)}, & x \in (\ell, +\infty). \end{cases} \tag{19}$$

with K_x in (15), $\sigma \geqslant 0$, and $\sigma^2 = k_y^2 - k^2$. At order 0 (corresponding to $\mathcal{B}_{\mathrm{M}} = \mathcal{C}_{\mathrm{M}} = 0$) which gives already very satisfactory results in the nonradiative region as shown in Fig. 4, by applying (8) at $x = \ell$, the effective dispersion relations of these guided waves read as

$$\mathrm{SPPs}\begin{cases} s : \sigma = \xi K_x \tan(K_x \ell), \\ a : \sigma = -\xi K_x \tan^{-1}(K_x \ell). \end{cases} \tag{20}$$

For M = 0, we recover the classical dispersion of SPPs, $\sigma = \xi k \tan(k\ell)$ and $\sigma = -\xi k \tan^{-1}(k\ell)$, for sound-rigid arrays pierced with holes [40,41], of which the homogenized version has been studied in [42] (see also [29] Â in the context of water waves). As it should be, the guided waves coincide with solutions of the scattering problem with diverging scattering coefficients (r, t) in (16) in the nonradiative region (for $k_x = i\sigma$). Accordingly, in Figs. 2 and 4, the SPP branches were already visible by means of the divergence of r (dark red lines) for $|k_y| > k$. From M = 0 to 0.5 the most striking features in the spectra are related to the inclination of the lines along which $r = 0$ (dark blue lines) by the equation of the lines D_m:

$$D_m : \quad k \simeq \mathrm{M}k_y + \sqrt{1-\mathrm{M}^2}\,\frac{m\pi}{2\ell}, \tag{21}$$

where $m \neq 0$ integer and in Fig. 4, $m = \pm 1, 2, 3, 4, 5$ are visible for M = 0.5 ($m = 1, 2, 3$ for M = 0). From (16), these lines D_m coincide with the asymptotes of the s- and a-SPP branches (labeled s_m and a_m) far enough from the radiative line $k_y = k$, where the increase in σ must be accompanied by

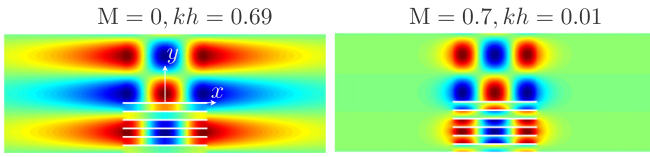

FIG. 6. SPP redshift. The SPP with $k_y h = -0.7$ is generated at the working frequency $kh = 0.69 \sim |k_y h|$ in the unmodulated grating while it is generated at almost vanishing frequency $kh = 0.01$ in the modulated grating for $\mathrm{M} = 0.7$ ($2\ell = 10h$). In each panel, the fields for $y < 0$ correspond to direct numerics and for $y > 0$ they correspond to the model (14).

large values of $\tan K_x \ell$ (m odd) or large values of $\tan^{-1} K_x \ell$ (m even).

A direct consequence of (21) is the capacity of the modulation M to produce the same wave number k_y of unmodulated SPP at fully controlled, lower or higher, working frequencies k. Such a blueshift, visible for $k_y > 0$, has been observed in [37] in time-varying array of split-ring resonators. The redshifts for $k_y < 0$ are even more impressive as they can drive to zero the working frequencies producing SPPs with large wave number k_y (in Fig. 4, s_0 to a_1). This is illustrated in Fig. 6 where we report SPP fields with $k_y h = -0.7$ for $\mathrm{M} = 0$ and 0.7. For $\mathrm{M} = 0$ the s_1 branch is close to the radiative limit line resulting in a weakly confined SPP ($k \simeq |k_y|$ hence $\sigma \sim 0$); for $\mathrm{M} = 0.7$, on the contrary, the frequency is shifted to $kh = 0.01$ resulting in a strongly confined SPP (in both cases, $2\ell = 10h$). On Fig. 6, we take the opportunity to comment on the meaning of the homogenized solution (14), or equivalently (18) and (19), which is reported in Fig. 6 for $y > 0$ (and numerical solution is reported for $y < 0$). As it should be, the homogenized solution in the grating provides a continuous picture of the actual one.

B. Accumulation of space-time modulated SPPs

Classical, i.e., unmodulated, SPPs have a unique solution $k_y(k) > 0$ at frequency k. From Fig. 4, we already know that this is no longer the case when the grating is modulated; we observe multiple branches and the number of these branches in a given interval of k_y increases without limit when M tends to 1, from (21). We will see that their number is in fact limited by the appearance of higher diffraction orders with real k_n given by (10) in the region where the 0 mode is evanescent; besides, the appearance of propagating modes transforms the SPPs in time-modulated SPPs excitable through scattering.

To begin with, we report in Fig. 7 the branches of the SPPs calculated numerically for $kh = 0.05$ and 0.2 increasing M [the agreement with the model (16) is exemplified in Fig. 8]. The associated mode 0 at the frequency k is evanescent except in a small region $k < |k_y|$; however, from (10), the modes $n = \pm 1$ appear for

$$\mathrm{PM}_{\pm 1}: \quad \mathrm{M} > 1 \pm (k_y - k)\frac{h}{2\pi}, \tag{22}$$

for $0 > k_y > -k$ ($n = 1$) and for $0 < k < k_y$ ($n = -1$). In the same way, the interference orders $n = \pm 2$ become propagating for $\mathrm{M} > 1 \pm (k_y - k)\frac{h}{4\pi}$.

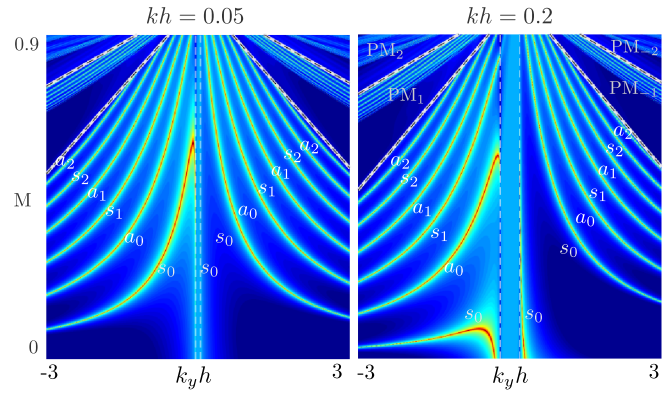

FIG. 7. Dispersion of the modulated SPPs against M for $kh = 0.05$ and 0.2 ($2\ell = 10h$); the mode 0 is propagating within the small region $|k_y h| < |kh|$. In the region $\mathrm{PM}_{\pm 1}$ the mode $n = \pm 1$ is propagating while the mode 0 is evanescent; in the region $\mathrm{PM}_{\pm 2}$ the modes $n = \pm 1$ and ± 2 are propagating while the mode 0 is evanescent.

Now in the limit of the low frequency $kh \sim 0$, the number N of SPP branches is, from (21), given by the condition $N \leqslant (2k_y\ell/\pi)\,\mathrm{M}/\sqrt{1-\mathrm{M}^2}$ (for $k_y > 0$) and it is limited in practice by the appearance of the higher diffraction order (the mode $n = -1$), hence, from (22) $0 < k_y h < 2\pi(1 - \mathrm{M})$. As a consequence, the number N of branches accumulated at given M is given by

$$N \sim \frac{4\ell}{h}\,\mathrm{M}\sqrt{\frac{1-\mathrm{M}}{1+\mathrm{M}}}, \tag{23}$$

which tells us that N is maximum for $\mathrm{M} \simeq 0.6$, in good agreement with the observation of Figs. 7 and 8 ($N \sim 1.2\ell/h = 6$ for $2\ell = 10h$).

We end this discussion by noticing branches with large, but *finite*, scattering values in the regions $\mathrm{PM}_{\pm 1}$ and $\mathrm{PM}_{\pm 2}$. This is the signature of time-modulated quasi-SPPs, that is to say, guided waves excitable through scattering. In particular, while true SPPs are associated with diverging scattering coefficient (in the numerics, this means that the maximum of r, or of t, is only limited by the discretization of k_y), quasi-SPPs have smooth variations of (r, t) with well-defined maxima. To demonstrate the leakage of the quasi-SPPs, we choose such a maximum in PM_2 region ($kh = 0.2$, $k_y h = -1.53$, $\mathrm{M} = 0.9$ in Fig. 7). This quasi-SPP can be excited by a propagating wave at frequency ω^{inc} if the pair (k, k_y) at frequency $\omega = ck$

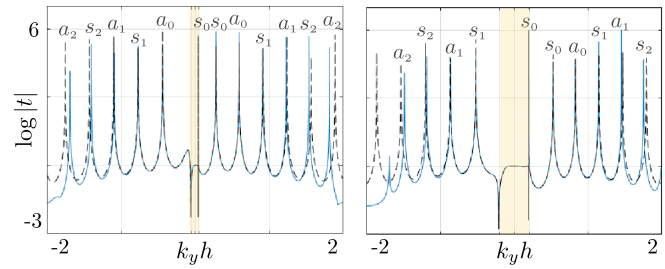

FIG. 8. Profiles from Fig. 7 at $\mathrm{M} = 0.7$ from direct numerics (plain blue line) and from the homogenized solution (16) (dashed black line).

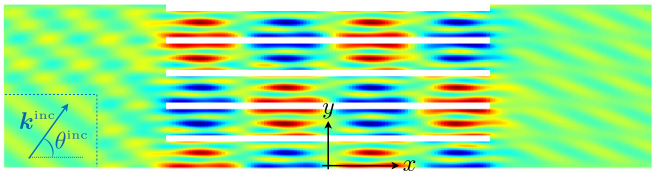

FIG. 9. φ field of the time-modulated quasi-SPP excited by an incident wave at frequency ω^{inc}; the inset shows the incident wave (mode 0). The quasi-SPP is associated to the frequency $\omega = \omega_{-1}$ [mode $n = -1$ in (24)]. The wave at frequency ω_1 is propagating [mode $n = 1$ in (24)], resulting in two propagating modes, 0 and 1, in reflection and transmission.

coincides with one of the pairs $(k_n, k_{y,n})$ of the modes n at $\omega_n = ck_n$. Denoting $k^{inc} = \omega^{inc}/c$, these modes are characterized by

$$k_n h = k^{inc} h + 2n\pi \mathrm{M}, \quad k_{y,n} h = k_y^{inc} h + 2n\pi, \tag{24}$$

at frequency $\omega_n = k_n/c$ (with n integer) [35]. We thus consider the propagating wave at $k^{inc}h = kh + 2\pi\mathrm{M} = 0.58$ [$n = -1$ in (24)] and incidence $\theta^{inc} = 54.3^\circ$ (with $\sin\theta^{inc} = k_y^{inc}/k^{inc}$ and $k_y^{inc}h = k_y h + 2\pi = 0.47$). The result is shown in Fig. 9 revealing the pattern of the time-modulated quasi-SPP at frequency ω with large amplitude in the grating, excited by an incident wave at frequency ω^{inc}. In the reported case, we observe also an additional diffraction order (mode 1) at higher frequency ($k_1 h = 11.5$, $k_{y,1}h = 11.0$) interfering with the incident wave in reflection and transmission.

V. SCATTERING PROPERTIES

In this section, we focus on the scattering properties of an incident propagating wave by a modulated metagrating. So, in the following, we denote θ the incident angle with $k_x = k\cos\theta$ and $k_y = k\sin\theta$. In particular, we will look at the effect of the M modulation on the perfect transmission conditions at the Brewster incidence angle and Fabry-Perot–type resonances, termed extraordinary acoustic transmission (EAT) for spatially modulated gratings only, see, e.g. [27,43].

A. Modulated EAT

The effective medium theory has become classical for predicting EATs through unmodulated rigid gratings [28,44]. At order 0 [$\mathcal{B} = \mathcal{C} = 0$ in (16) and (17)], perfect transmission is expected at the Brewster incidences $\theta_B^{\pm}$ realizing impedance matching condition whatever the frequency, with

$$\sin\theta_B^{\pm} = \frac{\mathrm{M}\xi^2 \pm (1-\mathrm{M}^2)\sqrt{1-\xi^2}}{1-\mathrm{M}^2(1-\xi^2)}, \tag{25}$$

and at Fabry-Pérot resonances $2K_x\ell = n\pi$ (n integer) whatever the incident angle, hence, $k = k_{FP}$ with

$$k_{FP} = \frac{\sqrt{1-\mathrm{M}^2}}{1-\mathrm{M}\sin\theta}\frac{n\pi}{2\ell}. \tag{26}$$

We report in Fig. 10 the reflection spectra $|r_{num}|$ against θ and M ($kh = 1$ and $\xi = 0.2$ or 0.8). We notice that the predictions

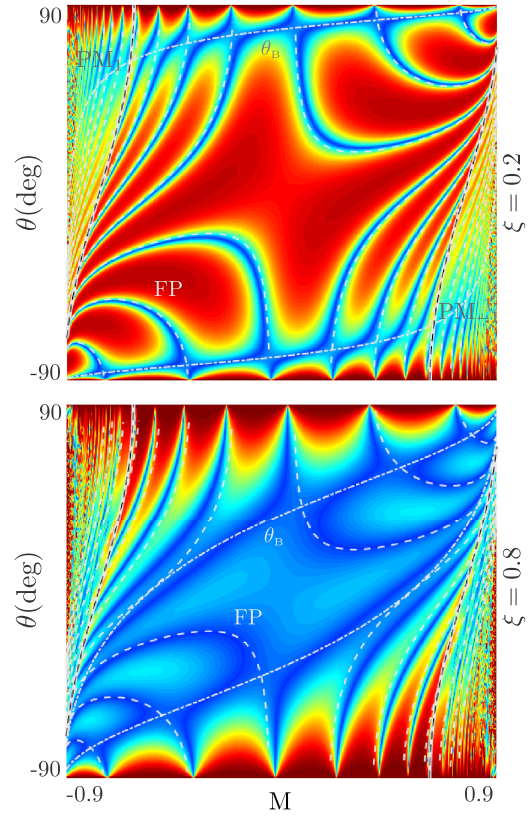

FIG. 10. Reflection spectra against θ and M ($kh = 1$, $\ell = 10h$). The gray lines show the EATs at Brewster angles (25) (dashed-dotted) and FP resonances (26) (dashed) given by the model at order 0.

(25) and (26) give a good qualitative picture of the occurrence of EATs. However, they are quantitatively imperfect, especially in the regions where the Brewster and FP curves intersect. This leads to a fairly high relative error of about 30% of the model at order 0. In comparison, the model at order 1 remains very accurate with a relative error lower than 5%; this was already visible on Fig. 5 in the radiative region. The models at orders 0 and 1 differ only in the effects of the evanescent field at the extremities of the grating (8). We already know that these boundary layer effects are responsible for an added length that can slightly shift the frequencies of the FPs [36]; we will see that they become an essential ingredient in determining whether the impedance of the grating can be tuned to that of the surrounding air.

B. Effect of boundary layers on EATs

From a physical point of view, the presence of boundary layers limits the ability of a stratified medium to be matched in impedance with the surrounding air. This difficulty can become critical and requires the use of models at higher order [38,45,46]. Here, a strong evanescent field is favored by the occurrence of FP resonances and according to (17) it is also favored by a strong modulation. Accounting for this evanescent field provides a perfect transmission condition, from (16) and (17), when the real part of $(Z_s Z_a^*)$ vanishes, i.e.,

$$k^2 A(\theta) B(K_x) = \varepsilon C(k,\theta), \tag{27}$$

where $k^2A(\theta) = (\xi^2 K_x^2 - k_x^2)$, $B(K_x) = \tan 2K_x\ell$, and $C(k,\theta) = 2\xi K_x(\mathcal{C}_\mathrm{M} + k_x^2\mathcal{B}_\mathrm{M})$. The right-hand term in (27) is the contribution at order 1 in $\varepsilon = kh$. The classical homogenized model at order 0 neglects this contribution and so it predicts (25) for $A(\theta) = 0$ and (26) for $B(K_x) = 0$. From the complete condition (27), this obviously becomes problematic when let us say $A(\theta) \sim \varepsilon^2$ which makes it impossible for the condition $B(K_x) \sim 0$ to occur simultaneously. The realization of perfect transmissions is therefore a more subtle interplay between the resonances of the grating and the evanescent field they generate. They are given by

$$\frac{\tan 2K_x\ell}{2K_x\ell} = \frac{h}{\ell}\, g(\theta), \tag{28}$$

where

$$g(\theta) = \frac{\xi}{\sqrt{1-\mathrm{M}^2}} \frac{\mathcal{C}(\sin\theta - \mathrm{M})^2 + \mathcal{B}\cos^2\theta(1-\mathrm{M}^2)}{\xi^2(1-\mathrm{M}\,\sin\theta)^2 - (1-\mathrm{M}^2)\cos^2\theta}, \tag{29}$$

[which is equivalent to (27)] and (28) indeed faithfully reproduces the EATs observed in Fig. 10.

Finally, we note that (28) provides conditions for which perfect transmission is not possible. Indeed, the function $g(\theta)$ in (29) takes all values in $\mathbb{R}$ except the values in the interval (g^-, g^+), with

$$g^- = -\frac{\mathcal{B}\xi}{(1-\xi^2)\sqrt{1-\mathrm{M}^2}} < 0, \quad g^+ = \frac{\mathcal{C}}{\xi\sqrt{1-\mathrm{M}^2}} > 0,$$

(see Appendix C). Therefore, perfect transmissions are prevented in regions where

$$\frac{\tan 2K_x\ell}{2K_x\ell} \in \frac{h}{\ell}(g^-, g^+), \tag{30}$$

which includes in particular the FP resonances at $2K_x\ell = n\pi$, $n \neq 0$, predicted by the model at order 0. To illustrate these effects, we plot in Fig. 11 the reflection spectra as functions of kh and θ for a relatively thin $\ell = h$ grating. The model at order 0 gives only an approximate prediction on the locations of perfect transmission, resulting in poor overall agreement. In contrast, the model at order 1 faithfully reproduces reality and seems to be limited only by the appearance of a new propagation mode.

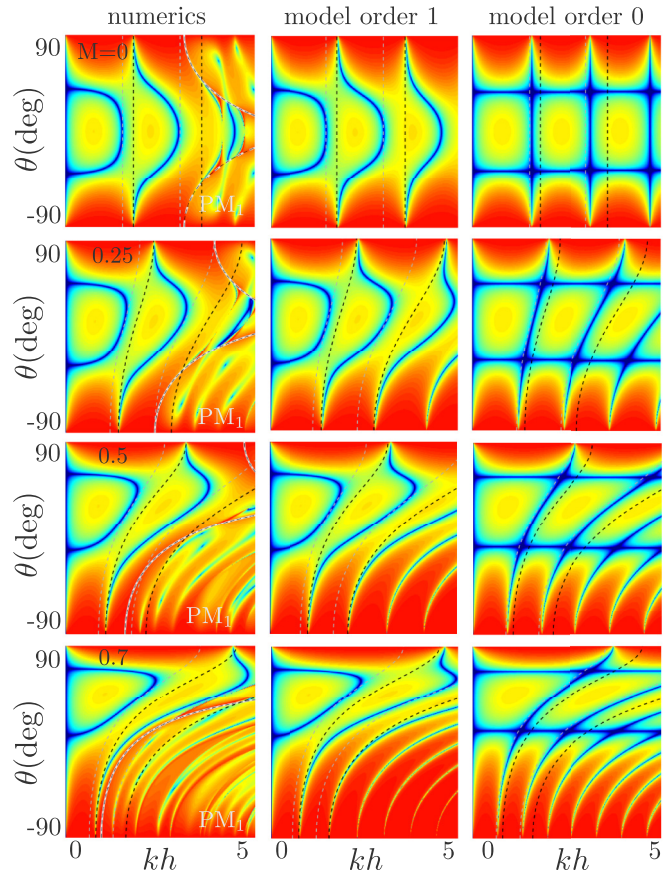

FIG. 11. Reflection spectra in the (k,θ) plane for $\ell = h, \xi = 0.8$. The bounds (30) in-between which perfect transmission is prevented are shown in gray dashed lines (light and dark, respectively).

VI. NEGATIVE REFRACTION AND PERFECT TRANSMISSION OF BEAMS

We now move to the scattering of an incident beam by our modulated gratings and we inspect its ability to control the energy flow. Inside the grating, we have shown in Sec. III A that the group velocity differs in general from the phase velocity, and it tells us that the energy is forced to flow along the direction $\alpha = \sin^{-1}\mathrm{M}$ [see (13) together with (12)], whatever the beam incidence θ. This is similar with the findings of [28,29] who focused on unmodulated gratings with plates tilted of an angle α; expectedly, we shall see that the analogy is partial only, essentially because these unmodulated gratings are nonsymmetric and reciprocal while our modulated gratings are symmetrical and nonreciprocal.

Outside the grating, the wave number is k and the incidence θ; the group and phase velocities are identical with $\boldsymbol{v}_p = \boldsymbol{v}_g = c(\cos\theta, \sin\theta)$. Inside the grating, the wave number is K and the refraction angle Θ. With $K_y = k_y = k\sin\theta$, we have

$$K = k\sqrt{1+\delta^2}, \quad \tan\Theta = \frac{\tan\alpha - \delta}{1+\delta\tan\alpha},$$

where

$$\delta = \frac{\sin\alpha - \sin\theta}{\cos\alpha},$$

from Sec. III A, and the group and phase velocities are given by (13). This tells us that for $\theta = \alpha$ ($\delta = 0$), the group and phase velocities inside the grating are equal; besides, they are equal to the group and phase velocities outside the grating. With in addition $K = k$ and $\Theta = \theta$, the wave transmitted in the grating has exactly the same properties as the incident wave. This is illustrated in Fig. 12 for a grating modulated at $\mathrm{M} = 0.7$: The beam is not deviated and the waves inside and outside the grating have the same characteristics. Expectedly however, a noticeable reflection occurs due to the impedance mismatch between the two media. In [29], unmodulated grating with zero thickness plates was shown to produce perfect beam transmission due to impedance matching and this is expected since the wave direction is that of the tilted plates. Interestingly, we shall see that the result holds for our modulated grating which is less intuitive.

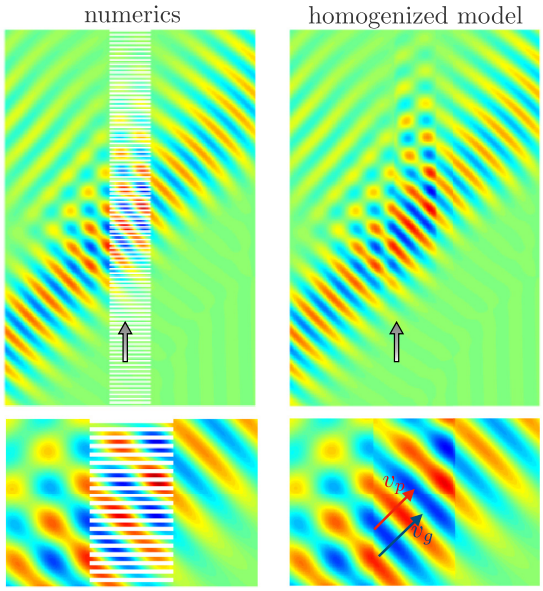

FIG. 12. Scattering of a beam at incidence $\theta = \alpha = 44.72^\circ$ by a modulated grating ($\xi = 0.5$, $2\ell = 10h$, $kh = 1$).

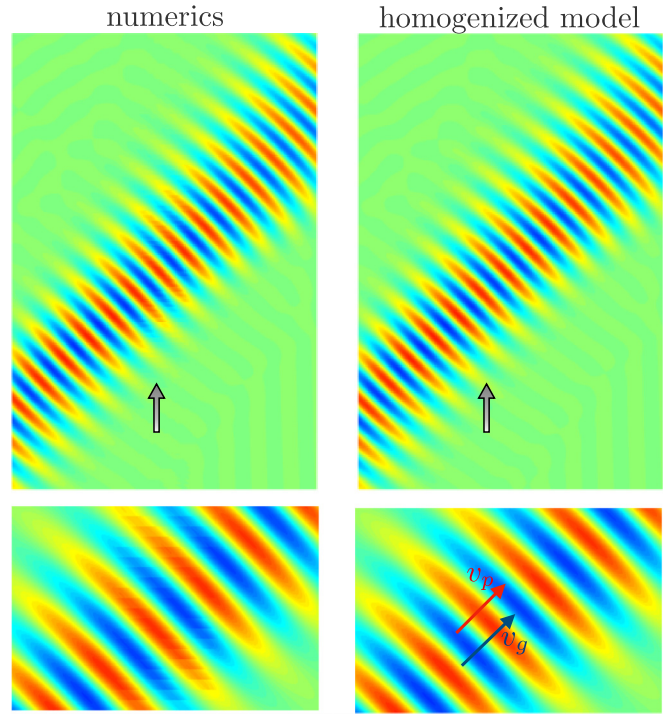

FIG. 13. Perfect beam transmission for $\xi = 1$ and $\theta = \theta_B = \alpha$. Same representation as in Fig. 12.

As discussed in the previous section, impedance matching is made difficult because of boundary layer effects but is it possible to remove these effects? This implies that the boundary layer parameters vanish, $\mathcal{B}_M = \mathcal{C}_M = 0$ in (17). It appears then that one can produce $\mathcal{B}_M = 0$ for $\xi = 1$ which was already true for an unmodulated grating and one can also produce $\mathcal{C}_M = 0$ if $M = \sin\theta$. This incidence corresponds precisely to the Brewster incidence (25) predicted at order 0 and which now holds also at order 1. The cancellation of the tuned beam reflection by the grating modulation is confirmed in Fig. 13. In the numerics, we set $\xi = 1 - 10^{-a}$ with increasing a and we obtain $|r_{num}| \sim 10^{-a}$ up to the numerical error for $a = 16$. It is interesting to note that this is also valid for the evanescent modes, suggesting that the result could be exact as for the tilted plate case [29].

In [28,29], it is shown that the refraction in a grating of tilted plates is negative as soon as $\theta\alpha < 0$. Moreover, the grating is equivalent to an anisotropic (and nonsymmetric) effective medium for which the general result $r(-\theta) = r(\theta)$ applies (see, e.g., [47]); this property leads to the unintuitive result that at incidence $\theta = -\alpha$ (and still $\xi = 1$), the negative refraction is accompanied by perfect transmission. For our modulated gratings, we find in the same way a negative refraction as soon as $\theta\alpha < 0$ since θ and α correspond to the beam directions in air and in the grating (which are given by the directions of the group velocities). However, the modulated grating cannot be assimilated to a classical anisotropic homogeneous slab (with continuity conditions at its extremities), hence, the equal reflection at $\pm\theta$ is lost in particular because $\mathcal{C}_M$ in (17) cannot be canceled for both $\pm k_y$. Another way to understand this difference is to use the nonreciprocity of the modulated grating. As the system is symmetric, nonreciprocity implies that the scattering process is not invariant under the transformation $(k_x, k_y) \to (k_x, -k_y)$ which is visible from Eqs. (15)–(17), hence under the transformation $\theta \to -\theta$ [and this is why $r(\pm\theta)$ differ]. Figure 14 illustrates the negative refraction of the beam in the grating. On these figures, we have plotted for comparison the result given by the model at order 1. As we had observed on Fig. 6, the model offers us a

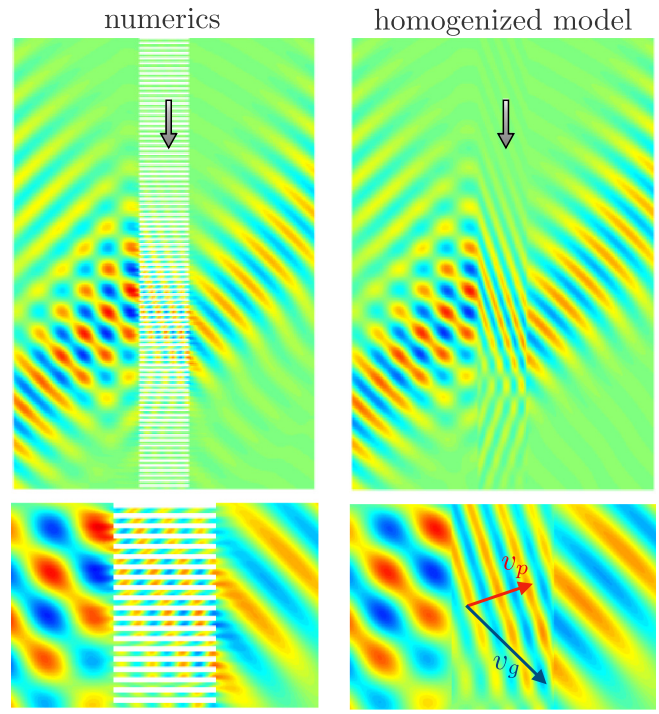

FIG. 14. Negative refraction of the beam for $\theta = -\alpha$ and nonreciprocal propagation (by comparison with Fig. 12). Here $v_p = 0.45c$ and $\Theta = 18.66^\circ$.

continuous version of the field in the grating and it captures the effects of the evanescent field in the jump conditions (8) which produce discontinuities (locally, at the interfaces) of the field and of its normal derivative (except for Fig. 13 which does not have them).

VII. CONCLUSION

We have analyzed the effect of space-time modulations on sound rigid gratings in the light of a model that captures propagation effects through an equivalent effective medium and boundary layer effects through nontrivial transmission conditions. Beyond the raw predictive strength of this model, which was illustrated by comparison with direct numerical solutions, explicit solutions were obtained for modulated SPPs and EAT. We have shown that the predictions of a model at order 0 are very qualitative while the model at order 1 accurately captures the complexity of the spectra, both models being nevertheless limited to the regime involving a single diffraction order.

The present analysis applies to analogous space-time modulated systems in electromagnetism such as laminated arrays alternating dielectrics, metals, or a mixture of both, a number of which have been analyzed using models at order 0. It also applies with some modifications to modulated metasurfaces for which boundary layer effects become dominant (and propagation negligible). Finally, we have referred to analyses carried out for unmodulated arrays formed by inclined rigid plates. It would be interesting to understand how these already rich results are modified when time modulation is added.

ACKNOWLEDGMENTS

K.P. acknowledges support of the Agence Nationale de la Recherche, France (Grant No. ANR-19-CE08-0006), and of the Agence de l'Innovation de Défense, France, from the Direction Générale de l'Armement (Grant No. 2019 65 0070).

APPENDIX A: FROM CONSERVATION LAWS TO SPACE-TIME MODULATION

We provide here a derivation of Eqs. (1)–(5) governing the actual space-time modulated problem starting with the classical conservation laws of mass and linear momentum. We consider a volume control element Ω whose boundary $\partial\Omega = \Gamma \cup \Gamma_v$ is made of a fixed external boundary Γ and internal moving lines of discontinuities Γ_v associated to the space-time modulations (Fig. 15). The balances of mass and of momentum in Ω read as

$$\begin{aligned}\frac{d}{dt}\int_\Omega \rho_{\rm t}\,d\boldsymbol{r} &= \int_{\Gamma_v} j\,d\ell - \int_\Gamma \rho_{\rm t}\boldsymbol{u}_{\rm t}\cdot\boldsymbol{n}\,d\ell,\\ \frac{d}{dt}\int_\Omega \rho_{\rm t}\boldsymbol{u}_{\rm t}\,d\boldsymbol{r} &= -\int_{\Gamma_v}\boldsymbol{t}\,d\ell - \int_\Gamma p_{\rm t}\boldsymbol{n}\,d\ell,\end{aligned} \tag{A1}$$

where $\rho_{\rm t}$, $p_{\rm t}$, and $\boldsymbol{u}_{\rm t}$ are the total mass density, pressure, and velocity of the air; next, j denotes the external flux of mass through Γ_v and $\boldsymbol{t}$ denotes the action force per unit length exerted by the air on Γ_v (these two terms are unknown at this stage and their values will be deduced in order to ensure the space-time modulation). Recalling that the lines of discontinuity Γ_v move at the velocity $\boldsymbol{v}$, the application of the Reynolds

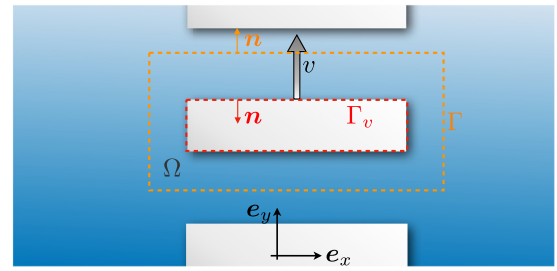

FIG. 15. Volume control element Ω in which the conservation laws (A1) are written. The boundary is $\partial\Omega = \Gamma \cup \Gamma_v$ with Γ a fixed external boundary and Γ_v made of internal moving lines of discontinuities associated to the space-time modulations.

transport theorem to the equations (A1) provides the relations

$$\begin{aligned}&\int_\Omega\left(\frac{\partial\rho_{\rm t}}{\partial t} + \mathrm{div}(\rho_{\rm t}\boldsymbol{u}_{\rm t})\right)d\boldsymbol{r} + \int_{\Gamma_v}\rho_{\rm t}(\mathbf{v}-\boldsymbol{u}_{\rm t})\cdot\boldsymbol{n}\,d\ell\\ &\quad= \int_{\Gamma_v} j\,d\ell,\\ &\int_\Omega\left(\rho_{\rm t}\frac{\partial\boldsymbol{u}_{\rm t}}{\partial t} + \boldsymbol{\nabla}p_{\rm t}\right)d\boldsymbol{r} + \int_{\Gamma_v}\rho_{\rm t}\boldsymbol{u}_{\rm t}(\mathbf{v}-\boldsymbol{u}_{\rm t})\cdot\boldsymbol{n}\,d\ell\\ &\quad= \int_{\Gamma_v}(p_{\rm t}\boldsymbol{n}-\boldsymbol{t})d\ell.\end{aligned} \tag{A2}$$

As the equations above are true for any domain Ω, we deduce the local set of equations

$$\frac{\partial\rho_{\rm t}}{\partial t} + \mathrm{div}(\rho_{\rm t}\boldsymbol{u}_{\rm t}) = 0, \quad \rho_{\rm t}\frac{\partial\boldsymbol{u}_{\rm t}}{\partial t} = -\boldsymbol{\nabla}p_{\rm t}, \tag{A3}$$

along with the values of the mass flux j and action force $\boldsymbol{t}$ at the moving lines of discontinuities

$$j = \rho_{\rm t}(\boldsymbol{v}-\boldsymbol{u}_{\rm t})\cdot\boldsymbol{n}, \quad \boldsymbol{t} = p_{\rm t}\boldsymbol{n} - \rho_{\rm t}\boldsymbol{u}_{\rm t}(\boldsymbol{v}-\boldsymbol{u}_{\rm t})\cdot\boldsymbol{n}. \tag{A4}$$

Now, we linearize the problem for small acoustic perturbations (the equilibrium being the air at rest with mass density ρ and pressure $p_{\rm e}$); introducing $\eta \ll 1$, we have $\rho_{\rm t} = \rho + \eta\rho'$, $p_{\rm t} = p_{\rm e} + \eta p$ with and $\boldsymbol{u}_{\rm t} = \eta\boldsymbol{u}$. On the one hand, the linearization of (A3) provides the usual (local) equations of conservation of mass and linear momentum for the acoustic perturbation after introduction of the acoustic pressure $p = c^2\rho'$ which defines the acoustic velocity c. On the other hand, the linearization of (A4) provides the boundary condition we are looking for. Namely, from the first equation in (A4) we obtain at the dominant order

$$j = \rho\boldsymbol{v}\cdot\boldsymbol{n}, \tag{A5}$$

and at the next order

$$\boldsymbol{u}\cdot\boldsymbol{n} = \boldsymbol{v}\cdot\boldsymbol{n}\frac{p}{\rho c^2}. \tag{A6}$$

The relation (A5) tells us that the space-time modulation in our configuration is provided by a mass injection ($\boldsymbol{n} = \boldsymbol{e}_y$, $j > 0$) or a mass withdrawal ($\boldsymbol{n} = -\boldsymbol{e}_y$, $j < 0$) at the moving boundary by an external process [8]; the resulting boundary condition (A6) links the acoustic pressure and velocity through the relation announced in (5). Note that such boundary condition is used in [3] from compatibility relations; it is

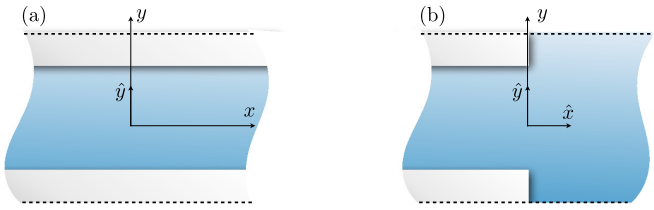

FIG. 16. (a) Unit cell used in the homogenization of the bulk, (b) Unit cell used for the homogenization of the transmission conditions.

also a relation similar to Rankine-Hugoniot condition between two fluids in the presence of a line of discontinuity. Finally, from the second equation in (A4), assuming that $\boldsymbol{t} = \boldsymbol{t}_e + \eta \boldsymbol{t}'$, we get at the dominant order the equilibrium force $\boldsymbol{t}_e = p_e \boldsymbol{n}$ exerted on the moving boundary and at the next order the acoustic force $\boldsymbol{t}' = p\boldsymbol{n} - \rho \boldsymbol{u}(\boldsymbol{v}\cdot\boldsymbol{n})$ which involves the velocity of the modulation.

APPENDIX B: ASYMPTOTIC HOMOGENIZATION

We report in this Appendix the derivation of the effective model given in (6)–(9). We first start by adimensionalizing the system (2), (3) in the moving frame as $(x, y) \to k(x, y - vt)$, $t \to \omega t$ and the fields $\boldsymbol{u} \to \boldsymbol{u}/c$, $p \to p/(Zc)$, $\varphi \to k\varphi/c$, which leads to the system

$$\boldsymbol{u} = \nabla\varphi, \quad p = -\left(\frac{\partial\varphi}{\partial t} - \mathrm{M}\frac{\partial\varphi}{\partial y}\right), \quad \mathrm{div}\boldsymbol{u} + \frac{\partial p}{\partial t} - \mathrm{M}\frac{\partial p}{\partial y} = 0, \tag{B1}$$

along with the boundary condition

$$(\boldsymbol{u} - \mathrm{M}p\boldsymbol{e}_y)\cdot\boldsymbol{n} = 0 \quad \text{on the rigid parts.} \tag{B2}$$

Following the adimensionalization, the periodicity becomes $\varepsilon = kh$ which is a small parameter in the subwavelength regime. The asymptotic analysis will be first conducted in the grating to find effective bulk equations and then at the interface between the grating and the air where effective jump conditions will be derived.

1. Effective equations

In the air and far from the interfaces at $x = \{0, k\ell\}$, the fields $(\boldsymbol{u}, p, \varphi)$ are simply expanded as

$$g = \sum_{i=0}^{\infty} \varepsilon^i g^i(\boldsymbol{r}, t), \quad g = \{\boldsymbol{u}, p, \varphi\}, \tag{B3}$$

with $\boldsymbol{r} = (x, y)$ describing the macroscopic variations of the fields. Accordingly, at any order i $(\boldsymbol{u}, p, \varphi)$ satisfy (B1).

In the grating, and still far from the interfaces at $x = \{0, k\ell\}$, the fields $(\boldsymbol{u}, p, \varphi)$ are expanded as

$$g = \sum_{i=0}^{\infty} \varepsilon^i \hat{g}^i(\boldsymbol{r}, \hat{y}, t), \quad \hat{g} = \{\hat{\boldsymbol{u}}, \hat{p}, \hat{\varphi}\}, \tag{B4}$$

where we introduce $\hat{y} = y/\varepsilon$ with $-\xi/2 < \hat{y} < \xi/2$ describing the microscopic variations at the scale of the periodic laminations [see Fig. 16(a)]. We define the fields of interest $(\boldsymbol{u}^i, p^i, \varphi^i)$ which are functions of $(\boldsymbol{r}, t)$ as

$$\boldsymbol{u}^i = \int_{-\xi/2}^{\xi/2} \hat{\boldsymbol{u}}^i d\hat{y}, \quad p^i = \int_{-\xi/2}^{\xi/2} \hat{p}^i d\hat{y}, \quad \varphi^i = \frac{1}{\xi}\int_{-\xi/2}^{\xi/2} \hat{\varphi}^i d\hat{y}, \tag{B5}$$

and the average process contains the meaning of the homogenization. In the following, we use (B4) in (B1) and identify the terms with same power in ε with the differential operator

$$\nabla \to \nabla_{\boldsymbol{r}} + \frac{\boldsymbol{e}_y}{\varepsilon}\frac{\partial}{\partial\hat{y}}.$$

a. The order 0

At the dominant order $1/\varepsilon$ in (B1), we have $\partial_{\hat{y}}\hat{\varphi}^0 = 0$, hence, from (B5) $\varphi^0 = \hat{\varphi}^0$. We also have $\partial_{\hat{y}}(\hat{u}_y^0 - \mathrm{M}\hat{p}^0) = 0$. Given the condition (B2) we deduce that

$$\hat{u}_y^0 - \mathrm{M}\hat{p}^0 = 0, \quad \forall\, \hat{y}. \tag{B6}$$

At the order ε^0 in (B1), we have $\hat{u}_y^0 = \partial_y\varphi^0 + \partial_{\hat{y}}\hat{\varphi}^1$ and $\hat{p}^0 = -\partial_t\varphi^0 + \mathrm{M}(\partial_y\varphi^0 + \partial_{\hat{y}}\hat{\varphi}^1)$. Combined with (B6) we obtain after integration over $\hat{y} \in (0, \xi)$

$$u_x^0 = \xi\frac{\partial\varphi^0}{\partial x}, \quad u_y^0 = -\frac{\xi\mathrm{M}}{1-\mathrm{M}^2}\frac{\partial\varphi^0}{\partial t}, \quad p^0 = -\frac{\xi}{1-\mathrm{M}^2}\frac{\partial\varphi^0}{\partial t} \tag{B7}$$

[$u_y^0 = \xi\hat{u}_y^0$ and $p^0 = \xi\hat{p}^0$ since $(\hat{u}_y^0, \hat{p}^0)$ do not depend on $\hat{y}$], and

$$\hat{\varphi}^1 = -\left(\frac{\mathrm{M}}{1-\mathrm{M}^2}\frac{\partial\varphi^0}{\partial t} + \frac{\partial\varphi^0}{\partial y}\right)\hat{y} + \varphi^1. \tag{B8}$$

Eventually, we use the equation of mass conservation at the order ε^0 in (B1). Since $(\hat{u}_y^0, \hat{p}^0)$ do not depend on $\hat{y}$, we deduce that $(\hat{u}_y^1 - \mathrm{M}\hat{p}^1)$ does not depend on $\hat{y}$ and using (B2)

$$\mathrm{div}_{\boldsymbol{r}}(\boldsymbol{u}^0 - \mathrm{M}p^0\boldsymbol{e}_y) + \frac{\partial p^0}{\partial t} = 0 \tag{B9}$$

(which holds for $\hat{u}_y^0$ and $\hat{p}^0$) and

$$\hat{u}_y^1 - \mathrm{M}\hat{p}^1 = 0, \quad \forall\, \hat{y}. \tag{B10}$$

b. The order 1

We use the forms of $(\hat{u}_y^1, \hat{p}^1)$ in (B1) at the order ε^1. As previously, by eliminating $\hat{\varphi}^2$, we obtain $\mathrm{M}\hat{u}_y^1 - \hat{p}^1 = \partial_t\hat{\varphi}^1$ which combined with (B10) provides the relations between the macroscopic fields

$$u_x^1 = \xi\frac{\partial\varphi^1}{\partial x}, \quad u_y^1 = -\frac{\xi\mathrm{M}}{1-\mathrm{M}^2}\frac{\partial\varphi^1}{\partial t}, \quad p^1 = -\frac{\xi}{1-\mathrm{M}^2}\frac{\partial\varphi^1}{\partial t}. \tag{B11}$$

Eventually, we use the equation of mass conservation in (B1) at the order ε^2 that we average on $\hat{y} \in (-\xi/2, \xi/2)$. Accounting for the condition (B2) $(\hat{u}_y^2 - \mathrm{M}\hat{p}^2) = 0$ results in

$$\mathrm{div}_{\boldsymbol{r}}(\boldsymbol{u}^1 - \mathrm{M}p^1\boldsymbol{e}_y) + \frac{\partial p^1}{\partial t} = 0. \tag{B12}$$

2. Effective interface jump conditions

The study of the behavior near interface at $x = 0$ (same procedure applies at $x = k\ell$) requires the introduction of the rescaled space variable $\hat{\boldsymbol{r}} = \boldsymbol{r}/\varepsilon$, with $\hat{\boldsymbol{r}} = (\hat{x}, \hat{y})$ and the associated elementary, or unit, cell $\mathcal{Y}$ of the interface [see Fig. 16(b)]. This representative cell is of infinite extent in the $\hat{x}$ direction and of thickness 1 in the $\hat{y}$ direction. In this domain, the fields $(\boldsymbol{u}, p, \varphi)$ are expanded as

$$g = \sum_{i=0}^{\infty} \varepsilon^i \hat{h}^i(y, \hat{\boldsymbol{r}}, t), \quad g = \{\boldsymbol{u}, p, \varphi\}, \ \hat{h} = \{\boldsymbol{v}, q, \psi\}, \quad \text{(B13)}$$

where $(\boldsymbol{v}^i, q^i, \psi^i)$ are $\hat{y}$-periodic functions for $\hat{y} < 0$. In (B13), we keep the macroscopic space variable y as it models the propagating behavior in the y direction. We shall use (B13) in (B1), with the differential operator

$$\boldsymbol{\nabla} \to \boldsymbol{e}_y \frac{\partial}{\partial y} + \frac{1}{\varepsilon} \boldsymbol{\nabla}_{\hat{\boldsymbol{r}}},$$

and identify the terms with same powers in ε. In this microscopic region, the inner expansions (B13) have to match the outer expansions (B3) and (B4), in the air and in the grating, respectively. This is done by means of matching conditions based on Taylor expansions (see, e.g., [48] for their derivation). Written at the dominant and first order for the velocities, they read as

$$\lim_{\hat{x}\to\pm\infty} \boldsymbol{v}^0 = \hat{\boldsymbol{u}}^0|_{0^\pm}, \quad \lim_{\hat{x}\to\pm\infty} \left(\boldsymbol{v}^1 - \hat{x} \frac{\partial \hat{\boldsymbol{u}}^0}{\partial x}\bigg|_{0^\pm} \right) = \hat{\boldsymbol{u}}^1|_{0^\pm}, \quad \text{(B14)}$$

with $\hat{\boldsymbol{u}}^i|_{0^-} = \boldsymbol{u}^i(0^-, y, t)$ and $\hat{\boldsymbol{u}}^i|_{0^+} = \hat{\boldsymbol{u}}^i(0^+, y, \hat{y}, t)$ for $i = 0, 1$. The same expressions hold for the matching on the pressure (the potential) by replacing formally $\boldsymbol{v}$ by q (ψ) and $\hat{\boldsymbol{u}}$ by $\hat{p}$ $(\hat{\varphi})$.

a. The order 0

We start with the terms in $1/\varepsilon$ in (B1), which already tells us that $\boldsymbol{\nabla}_{\hat{\boldsymbol{r}}} \psi^0 = \boldsymbol{0}$, hence, ψ^0 does not depend on $\hat{\boldsymbol{r}}$. From (B14), we deduce that φ^0 is continuous at $x = 0$ and

$$\psi^0 = \varphi^0(0, y, t). \quad \text{(B15)}$$

We also have the relation $\mathrm{div}_{\hat{\boldsymbol{r}}}(\boldsymbol{v}^0 - \mathrm{M} q^0 \boldsymbol{e}_y) = 0$, that we integrate over $\mathcal{Y}$ and obtain

$$0 = \lim_{\hat{x}\to+\infty} \int_{\hat{y}=0}^{\xi} v_x^0 d\hat{y} - \lim_{\hat{x}\to-\infty} \int_{\hat{y}=0}^{1} v_x^0 d\hat{y}$$

[accounting for the periodicity along $\hat{y}$ and (B2)]. Applying the matching condition (B14), we find

$$u_x^0(0^+, y, t) = u_x^0(0^-, y, t).$$

Therefore, we have continuity of the potential field and the velocity at the dominant order

$$[\![\varphi^0]\!] = 0, \quad [\![u_x^0]\!] = 0. \quad \text{(B16)}$$

b. The order 1

For simplicity, we introduce the fields $\boldsymbol{w}^0$ and K^0 defined by

$$\begin{aligned} &\boldsymbol{w}^0 = (\boldsymbol{v}^0 - \mathrm{M} q^0 \boldsymbol{e}_y), \\ &K^0 = \mathrm{M} \tfrac{\partial \varphi^0}{\partial t}\big|_0 + (1 - \mathrm{M}^2) \tfrac{\partial \varphi^0}{\partial y}\big|_0 = \mathcal{L}\varphi^0_{|0}. \end{aligned} \quad \text{(B17)}$$

From the relation pressure potential in (B1) at the order ε^0, and accounting for (B15), we have

$$q^0 = -\frac{\partial \varphi^0}{\partial t}\bigg|_0 + \mathrm{M}\left(\frac{\partial \varphi^0}{\partial y}\bigg|_0 + \frac{\partial \psi^1}{\partial \hat{y}} \right), \quad \text{(B18)}$$

satisfying the matching conditions

$$\begin{aligned} &\lim_{\hat{x}\to-\infty} q^0 = -\tfrac{\partial \varphi^0}{\partial t}\big|_0 + \mathrm{M} \tfrac{\partial \varphi^0}{\partial y}\big|_0, \\ &\lim_{\hat{x}\to+\infty} q^0 = -\tfrac{1}{1-\mathrm{M}^2} \tfrac{\partial \varphi^0}{\partial t}\big|_0 \end{aligned} \quad \text{(B19)}$$

[we have used (B7)]. We now move to the problem set on $(\boldsymbol{w}^0, \psi^1)$ in $\mathcal{Y}$. To do so, we use (B1) the conservation of the mass (at the order $1/\varepsilon$) and $\boldsymbol{v}^0$ (at the order ε^0) along with (B18), the boundary condition (B2) (at the order ε^0). This allows us to set the elementary problem on $(\boldsymbol{w}^0, \psi^1)$ solution to

$$\begin{aligned} &\mathrm{div}_{\hat{\boldsymbol{r}}} \boldsymbol{w}^0 = 0, \\ &\boldsymbol{w}^0 = \boldsymbol{\nabla}_{\hat{\boldsymbol{r}}} \psi^1 - \mathrm{M}^2 \tfrac{\partial \psi^1}{\partial \hat{y}} \boldsymbol{e}_y + K^0 \boldsymbol{e}_y, \\ &\boldsymbol{w}^0 \cdot \boldsymbol{n} = 0 \quad \text{on the rigid parts.} \end{aligned} \quad \text{(B20)}$$

The above system is complemented by the matching conditions using (B14) on $\boldsymbol{v}^0$. Using further (B19) and remembering that at $x = 0^-$, $\hat{\boldsymbol{u}}^0$ is given directly by (B1) and at $x = 0^+$, $\hat{\boldsymbol{u}}^0 = \boldsymbol{u}^0/\xi$ is given by (B7), we obtain

$$\lim_{\hat{x}\to-\infty} \boldsymbol{w}^0 = u_x^0|_0 \boldsymbol{e}_x + K^0 \boldsymbol{e}_y, \quad \lim_{\hat{x}\to+\infty} \boldsymbol{w}^0 = \frac{u_x^0|_0}{\xi} \boldsymbol{e}_x. \quad \text{(B21)}$$

The problem (B20), (B21) is linear with respect to K^0 and $u_x^0|_0$, hence, the solution can be expressed as

$$\psi^1 = u_x^0|_0 \, Q^1(\hat{\boldsymbol{r}}) + K^0 \, Q^2(\hat{\boldsymbol{r}}) + \tilde{\psi}^1(y, t), \quad \text{(B22)}$$

where Q^1 and Q^2 are elementary functions, periodic in $\mathcal{Y}^-$, that satisfy

$$\begin{aligned} &\tfrac{\partial^2 Q^1}{\partial \hat{x}^2} + (1 - \mathrm{M}^2) \tfrac{\partial^2 Q^1}{\partial \hat{y}^2} = 0, \\ &\lim_{\hat{x}\to-\infty} \boldsymbol{\nabla}_{\hat{\boldsymbol{r}}} Q^1 = \boldsymbol{e}_x, \quad \lim_{\hat{x}\to+\infty} \boldsymbol{\nabla}_{\hat{\boldsymbol{r}}} Q^1 = \tfrac{\boldsymbol{e}_x}{\xi}, \\ &\boldsymbol{\nabla}_{\hat{\boldsymbol{r}}} Q^1 \cdot \boldsymbol{n} = 0 \quad \text{on the rigid parts} \end{aligned} \quad \text{(B23)}$$

and

$$\begin{aligned} &\tfrac{\partial^2 Q^2}{\partial \hat{x}^2} + (1 - \mathrm{M}^2) \tfrac{\partial^2 Q^2}{\partial \hat{y}^2} = 0, \\ &\lim_{\hat{x}\to-\infty} \boldsymbol{\nabla}_{\hat{\boldsymbol{r}}} Q^2 = \boldsymbol{0}, \quad \lim_{\hat{x}\to+\infty} \boldsymbol{\nabla}_{\hat{\boldsymbol{r}}} Q^2 = -\tfrac{\boldsymbol{e}_y}{1-\mathrm{M}^2}, \\ &\boldsymbol{\nabla}_{\hat{\boldsymbol{r}}} Q^2 \cdot \boldsymbol{n} = -\tfrac{\boldsymbol{e}_y \cdot \boldsymbol{n}}{1-\mathrm{M}^2} \quad \text{on the rigid parts.} \end{aligned} \quad \text{(B24)}$$

From (B23) and (B24), we deduce that Q^1 and Q^2 at infinity should read as

$$Q^1 \underset{\hat{x}\to-\infty}{\sim} \hat{x}, \quad Q^1 \underset{\hat{x}\to+\infty}{\sim} \frac{\hat{x}}{\xi} + B, \quad \text{(B25a)}$$

$$Q^2 \underset{\hat{x}\to-\infty}{\sim} 0, \quad Q^2 \underset{\hat{x}\to+\infty}{\sim} -\frac{\hat{y}}{1-\mathrm{M}^2}, \quad \text{(B25b)}$$

where B is a boundary layer parameter. We shall see in Appendix B 3 that $B = \mathcal{B}/\sqrt{1-\mathrm{M}^2}$ where $\mathcal{B}$ is an effective parameter independent of M and which only depends on ξ. Note that since the problems (B23) and (B24) are defined up to a constant, we fix the constant to zero at $\hat{x} = -\infty$. As the geometry is symmetric with respect to $\hat{y} = \xi/2$, we have $Q^2(\hat{x}, \xi/2) = 0$ and hence no effective coefficient appears for Q^2, hence (B25b). Now making use of the matching conditions with ψ^1 in (B22) along with (B25a) and (B25b) and using further (B8), we obtain

$$[\![\varphi^1]\!] = Bu_x^0\big|_0. \tag{B26}$$

It remains to derive the jump condition on the normal velocity at the interface by integrating the equation of mass conservation in (B1) at the order ε^0, namely, $\mathrm{div}_{\hat{\boldsymbol{r}}}\boldsymbol{w}^1 + (\partial_t q^0 + \partial_y w_y^0) = 0$. Since the integration of each term makes diverging terms to appear, we will perform the integration on a finite domain $\mathcal{Y}_m = \mathcal{Y}_m^+ \cup \mathcal{Y}_m^-$ with $\mathcal{Y}_m^\pm = \{\hat{\boldsymbol{r}} \in \mathcal{Y} \mid \pm\hat{x} > 0, |\hat{x}| < \hat{x}_m\}$ with $\hat{x}_m > 0$ and consider the limit $\hat{x}_m \to \infty$. Using the Green theorem along with (B2) and (B14), we obtain

$$\int_{\mathcal{Y}_m} \mathrm{div}_{\hat{\boldsymbol{r}}}\boldsymbol{w}^1 d\hat{\boldsymbol{r}} \underset{\hat{x}_m\to\infty}{\sim} [\![u_x^1]\!] + \hat{x}_m\left(\frac{\partial u_x^0}{\partial x}\bigg|_{0^+} + \frac{\partial u_x^0}{\partial x}\bigg|_{0^-}\right). \tag{B27}$$

We have used that the terms $\partial_x u^0_{x|0^\pm}$ are obtained from the equation of mass conservation and the forms of (p^0, u_y^0) in (B1) at the order ε^0 in $\mathcal{Y}_m$, and using (B7) and (B9) in $\mathcal{Y}_m^+$. We obtain

$$\frac{\partial u_x^0}{\partial x}\bigg|_{0^+} = \frac{\xi}{1-\mathrm{M}^2}\frac{\partial^2\varphi^0}{\partial t^2}\bigg|_0,$$
$$\frac{\partial u_x^0}{\partial x}\bigg|_{0^-} = \frac{1}{1-\mathrm{M}^2}\left(\frac{\partial^2\varphi^0}{\partial t^2}\bigg|_0 - \mathcal{L}K^0\right).$$

With the operator $\mathcal{L} = [\mathrm{M}\partial_t + (1-\mathrm{M}^2)\partial_y]$, as in (B17), the second contribution reads as

$$\int_{\mathcal{Y}_m}\left(\frac{\partial q^0}{\partial t} + \frac{\partial w_y^0}{\partial y}\right)d\hat{\boldsymbol{r}} \underset{\hat{x}_m\to\infty}{\sim} \frac{\mathcal{L}K^0}{1-\mathrm{M}^2}\,C - \frac{\hat{x}_m}{1-\mathrm{M}^2}\left(\frac{\partial^2\varphi^0}{\partial t^2}\bigg|_0 (1+\xi) - \mathcal{L}K^0\right), \tag{B28}$$

where we have used q^0 from (B18) and w_y^0 from (B20) and (B22). We also used that Q^1 is an even function of $\hat{y}$ and we have introduced the finite integral

$$C = \int_{\mathcal{Y}^-}(1-\mathrm{M}^2)\frac{\partial Q^2}{\partial\hat{y}}d\hat{\boldsymbol{r}} + \int_{\mathcal{Y}^+}\left((1-\mathrm{M}^2)\frac{\partial Q^2}{\partial\hat{y}} + 1\right)d\hat{\boldsymbol{r}}. \tag{B29}$$

As for the constant B, we will show in Appendix B 3 that $C = \mathcal{C}/\sqrt{1-\mathrm{M}^2}$ where $\mathcal{C}$ is an effective parameter independent of M and which only depends on ξ. Gathering the contributions (B27) and (B28), the diverging terms in $\hat{x}_m$ cancel out and we obtain

$$[\![u_1^1]\!] = -\frac{\mathcal{L}^2\varphi^0_{|0}}{1-\mathrm{M}^2}\,C. \tag{B30}$$

3. Classical form of the elementary problems

The elementary problems in (B23) and (B24) can be put in a classical form independent of M by setting, with $\mathrm{c}_\alpha = \sqrt{1-\mathrm{M}^2}$,

$$\tilde{Q}^1(\tilde{x},\tilde{y}) = \mathrm{c}_\alpha\, Q^1(\tilde{x}/\mathrm{c}_\alpha, \tilde{y}), \quad \tilde{Q}^2(\tilde{x},\tilde{y}) = \mathrm{c}_\alpha^2\, Q^2(\tilde{x}/\mathrm{c}_\alpha, \tilde{y}).$$

Accordingly, $(\tilde{Q}^1, \tilde{Q}^2)$ satisfy (B23) and (B24) with $\mathrm{M} = 0$ (in particular they satisfy a Laplace equation). These problems are classical potential flow problems which depend only on ξ and they have been analyzed in [36]. Introducing $(\mathcal{B}, \mathcal{C})$ defined by

$$\tilde{Q}^1 \underset{\tilde{x}\to+\infty}{\sim} \frac{\tilde{x}}{\xi} + \mathcal{B}, \quad \mathcal{C} = \int_{\mathcal{Y}^-}\frac{\partial\tilde{Q}^2}{\partial\tilde{y}}d\tilde{\boldsymbol{r}} + \int_{\mathcal{Y}^+}\left(\frac{\partial\tilde{Q}^2}{\partial\tilde{y}} + 1\right)d\tilde{\boldsymbol{r}},$$

and identifying with (B25a) and (B29), we deduce that

$$B = \frac{\mathcal{B}}{\sqrt{1-\mathrm{M}^2}}, \quad C = \frac{\mathcal{C}}{\sqrt{1-\mathrm{M}^2}}, \tag{B31}$$

where the dependence of (B, C) on M is now explicit, and $\mathcal{B}$ and $\mathcal{C}$ depend on ξ only. Specifically, we have

$$\mathcal{B} = -\frac{1}{\pi}\log\left(\sin\frac{\pi\xi}{2}\right), \quad \mathcal{C} \simeq \frac{\pi\xi^2}{16}$$

[see [36] (note that in this reference, we used $p \to p/\xi$)].

4. Construction of the model at order 1

The final problem is set on a unique homogenized field $(\boldsymbol{u}, \varphi) = (\boldsymbol{u}^0, \varphi^0) + \varepsilon(\boldsymbol{u}^1, \varphi^1)$ which consists in collecting the first two order contributions of the expansions. We first remark that in the air for $x < 0$ and $x > k\ell$, the unique field satisfies the exact same wave equation than that in the initial system (B1). Next, in the region of the modulated grating, the unique field satisfies an effective wave equation consisting in a balance of mass

$$\mathrm{div}_{\boldsymbol{r}}\boldsymbol{u} + \frac{\partial p}{\partial t} - \mathrm{M}\frac{\partial p}{\partial y} = 0,$$

from (B9) and (B12), along with

$$\boldsymbol{u} = \xi\tfrac{\partial\varphi}{\partial x}\boldsymbol{e}_x - \tfrac{\xi\mathrm{M}}{1-\mathrm{M}^2}\tfrac{\partial\varphi}{\partial t}\boldsymbol{e}_y,$$
$$p = -\tfrac{\xi}{1-\mathrm{M}^2}\tfrac{\partial\varphi}{\partial t}$$

from (B7)–(B11). At the interface between the air and the grating, by gathering the contributions (B16) at order 0, (B26) and (B30) at order 1, and accounting for (B31), we obtain

$$[\![\varphi]\!] = \frac{\epsilon\mathcal{B}}{\sqrt{1-\mathrm{M}^2}}\,\overline{u_x}, \quad [\![u_x]\!] = -\frac{\epsilon\mathcal{C}}{(1-\mathrm{M}^2)^{3/2}}\,\mathcal{L}^2\overline{\varphi}.$$

Finally, going back to the reference frame and dimensional forms, we recover the effective model announced in (6) along with (3) and the transmission conditions (8).

5. Nonreciprocity

In this section, we come back to the homogenization recently proposed in [33] in the context of electromagnetic waves for dielectric materials, as the case a perfect electric conductor (PEC) we are considering in this study is a delicate limit. In the following, we set $Z = c = 1$ for simplicity. In

[33], the homogenization process ends up with a homogenized model in which the structure of the Maxwell $\mathrm{rot}\boldsymbol{E} = -\partial_t \boldsymbol{B}$, $\mathrm{rot}\boldsymbol{H} = \partial_t \boldsymbol{D}$, is preserved, while the constitutive relations between the four fields are those of bianisotropic media, namely,

$$\begin{aligned} \boldsymbol{D} &= \boldsymbol{\varepsilon}\boldsymbol{E} + ({}^t\boldsymbol{\chi} - i\,{}^t\boldsymbol{\kappa})\boldsymbol{H}, \\ \boldsymbol{B} &= \boldsymbol{\mu}\boldsymbol{H} + (\boldsymbol{\chi} + i\,{}^t\boldsymbol{\kappa})\boldsymbol{E}, \end{aligned} \tag{B32}$$

where $\boldsymbol{\varepsilon}$ and $\boldsymbol{\mu}$ are the permittivity and permeability dyadics, $\boldsymbol{\chi}$ and $\boldsymbol{\kappa}$ the nonreciprocity and chirality parameters [49]. In the present case, $\boldsymbol{\kappa} = \mathbf{0}$ and ${}^t\boldsymbol{\chi} = -\boldsymbol{\chi}$, which corresponds to nonreciprocal bianisotropy in moving media [49,50]. To relate with our problem in acoustics, we consider p polarization $\boldsymbol{H} = H(x, y)\boldsymbol{e}_z$ and a modulation along $\boldsymbol{e}_y$, for which

$$\boldsymbol{\chi} = \begin{pmatrix} 0 & 0 & \chi \\ 0 & 0 & 0 \\ -\chi & 0 & 0 \end{pmatrix}. \tag{B33}$$

This results in the following relations:

$$\partial_x E_y - \partial_y E_x + \partial_t B = 0, \tag{B34}$$

along with $\partial_y H = \partial_t D_x$ and $\partial_x H = -\partial_t D_y$ and

$$\begin{pmatrix} D_y \\ D_x \\ B \end{pmatrix} = \begin{pmatrix} \epsilon_\parallel & 0 & 0 \\ 0 & \epsilon_\perp & -\chi \\ 0 & -\chi & \mu_\perp \end{pmatrix} \begin{pmatrix} E_y \\ E_x \\ H \end{pmatrix}. \tag{B35}$$

Noticing that (3) and (6) can be written

$$\partial_x u_x + \partial_y u_y + \partial_t p = 0, \tag{B36}$$

$$\begin{pmatrix} \partial_x \varphi \\ \partial_y \varphi \\ p \end{pmatrix} = \begin{pmatrix} \frac{1}{\xi} & 0 & 0 \\ 0 & -\frac{1-\mathrm{M}^2}{\xi\,\mathrm{M}^2} & -\frac{1}{\mathrm{M}} \\ 0 & \frac{1}{\mathrm{M}} & 0 \end{pmatrix} \begin{pmatrix} u_x \\ u_y \\ -\partial_t \varphi \end{pmatrix}, \tag{B37}$$

(B34) and (B35) can be identified to (B36) and (B37) using

$$\begin{aligned} E_y &= u_x, \quad & E_x &= -u_y, \quad & B &= p, \\ D_y &= \partial_x \varphi, \quad & D_x &= -\partial_y \varphi, \quad & H &= -\partial_t \varphi, \end{aligned}$$

resulting in

$$\epsilon_\parallel = \frac{1}{\xi}, \quad \epsilon_\perp = -\frac{1-\mathrm{M}^2}{\xi \mathrm{M}^2}, \quad \mu_\perp = 0, \quad \chi = \frac{1}{\mathrm{M}}. \tag{B38}$$

We notice that $\epsilon_\perp$ and χ diverge as $\mathrm{M} \to 0$, which is expected. Indeed, when $\mathrm{M} = 0$, the inversion which results in (B37), namely from (6),

$$\begin{pmatrix} u_y \\ -\partial_t \varphi \end{pmatrix} = \begin{pmatrix} 0 & \mathrm{M} \\ \mathrm{M} & \frac{1-\mathrm{M}^2}{\xi} \end{pmatrix} \begin{pmatrix} \partial_y \varphi \\ p \end{pmatrix},$$

is not possible anymore due to the infinite anisotropy. Conducting the homogenization directly for a perfect electric conductor (PEC) provides $E_x = 0$ ($u_y = 0$ in acoustics) and the one-dimensional wave equation

$$\partial_x E_y + \xi\, \partial_t H = 0, \quad \partial_t E_y = -\xi\, \partial_x H.$$

Alternatively, (B35) can be recovered from [33] by assimilating formally a PEC (or a sound-rigid material) to a material with $\epsilon \to \infty$ (or $\rho \to \infty$) while keeping an arbitrary but finite value of c [42]. By doing so in [33], with $1/\epsilon_2 = \mu_2 = 0$ for a PEC (and for simplicity, one can use $\epsilon_1 = \mu_1 = 1$ and $c_1 = c_2 = 1$), (42–46) and (25–29) in this reference provide (B38) (and $\mu_\parallel = 0$). From (B34) and (B35) along with the relations $\partial_y H = \partial_t D_x$ and $\partial_x H = -\partial_t D_y$, we obtain the dispersion relation

$$\frac{\epsilon_\perp}{\epsilon_\parallel} K_x^2 + (K_y - \zeta k)^2 = \epsilon_\perp \mu_\perp k^2,$$

where $k = \omega/c$, which using (B38) provides (11). For $\mathrm{M} = 0$, the dispersion reduces to $K_x = \pm k$ as expected.

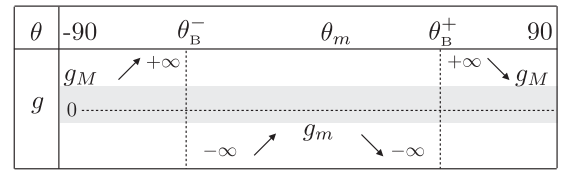

FIG. 17. Variation of g as a function of θ.

APPENDIX C: BREWSTER AND FABRY-PÉROT

Here, we provide additional (technical) information on the analysis used in Sec. V B. We note

$$g(\theta) = \frac{\xi}{\sqrt{1-\mathrm{M}^2}} \frac{a(\theta, \mathrm{M})}{b(\theta, \xi, \mathrm{M})},$$

with from (29), $a(\theta, \mathrm{M}) = \mathcal{C}(\sin\theta - \mathrm{M})^2 + \mathcal{B}\cos^2\theta(1 - \mathrm{M}^2)$ and $b(\theta, \xi, \mathrm{M}) = \xi^2(1 - \mathrm{M}\sin\theta)^2 - (1 - \mathrm{M}^2)\cos^2\theta$. The derivative of g with respect to θ is

$$\partial_\theta g = \frac{2\xi\sqrt{1-\mathrm{M}^2}}{b^2(\theta, \xi, \mathrm{M})} \mathrm{c}_\theta (1 - \mathrm{M}\mathrm{s}_\theta)[\mathcal{B}\xi^2 + \mathcal{C}(1 - \xi^2)](\mathrm{M} - \mathrm{s}_\theta),$$

whose sign is given by the sign of $(\mathrm{M} - \mathrm{s}_\theta)$ and we denote $\theta_m = \sin^{-1}\mathrm{M}$. The function g and $\partial_\theta g$ have poles which are precisely the Brewster angles $\theta_\mathrm{B}^\pm$ predicted by the homogenization at the order 0 [see (25)]. With the hierarchy $\theta_\mathrm{B}^- \leqslant \theta_m \leqslant \theta_\mathrm{B}^+$, for any ξ and M, we obtain the following table of Fig. 17, where $g_m = g(\theta_m, \xi, \mathrm{M})$ and $g_m = g(\pm 90^\circ, \xi, \mathrm{M})$ are given by

$$g_m = -\frac{\mathcal{B}\xi}{(1-\xi^2)\sqrt{1-\mathrm{M}^2}} \leqslant 0, \quad g_M = \frac{\mathcal{C}}{\xi\sqrt{1-\mathrm{M}^2}} \geqslant 0$$

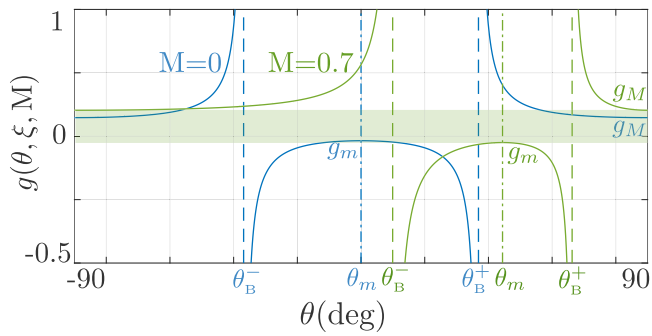

FIG. 18. Variations of $g(\theta, \xi, \mathrm{M})$ against θ for $\xi = 0.8$ and $\mathrm{M} = 0$ and 0.7.

[since $\mathcal{B} \geqslant 0$ and $\mathcal{C} > 0$ from (9)]. We obtain that g does not take values within the interval (g_m, g_M) (see Fig. 18). It follows that the condition for perfect transmission

$$\frac{\tan 2K_x\ell}{2K_x\ell} = \frac{h}{\ell}\, g(\theta, \xi, \mathrm{M}),$$

cannot be fulfilled when $\tan 2K_x\ell/(2K_x\ell)$ falls in this interval, and in particular for $2K_x\ell = n\pi$ which coincide with the perfect transmissions predicted by the homogenized model at the order 0. Instead, in this vicinity, we obtain

$$2K_x\ell - n\pi \simeq n\pi \frac{h}{\ell}\, g(\theta, \xi, \mathrm{M}).$$

[1] J.-C. Simon, Action of a progressive disturbance on a guided electromagnetic wave, IEEE Trans. Microwave Theory Techn. **8**, 18 (1960).

[2] A. Oliner and A. Hessel, Wave propagation in a medium with a progressive sinusoidal disturbance, IEEE Trans. Microwave Theory Techn. **9**, 337 (1961).

[3] K. A. Lurie, Effective properties of smart elastic laminates and the screening phenomenon, Int. J. Solids Struct. **34**, 1633 (1997).

[4] K. A. Lurie, The problem of effective parameters of a mixture of two isotropic dielectrics distributed in space-time and the conservation law for wave impedance in one-dimensional wave propagation, Proc. R. Soc. London, Ser. A **454**, 1767 (1998).

[5] I. Blekhman and K. A. Lurie, On dynamic materials, *Doklady Physics* (Nauka/Interperiodica, Moscow, 2000), Vol. 45, pp. 118–121.

[6] K. A. Lurie and S. L. Weekes, Wave propagation and energy exchange in a spatio-temporal material composite with rectangular microstructure, J. Math. Anal. Appl. **314**, 286 (2006).

[7] K. A. Lurie *et al.*, *An Introduction to the Mathematical Theory of Dynamic Materials*, Vol. 15 (Springer, Berlin, 2007).

[8] K. A. Lurie, On homogenization of activated laminates in 1D-space and time, Z. Angew. Math. Mech. **89**, 333 (2009).

[9] H. Nassar, X. Xu, A. Norris, and G. Huang, Modulated phononic crystals: Non-reciprocal wave propagation and Willis materials, J. Mech. Phys. Solids **101**, 10 (2017).

[10] L. Zhang, X. Q. Chen, R. W. Shao, J. Y. Dai, Q. Cheng, G. Castaldi, V. Galdi, and T. J. Cui, Breaking reciprocity with space-time-coding digital metasurfaces, Adv. Mater. **31**, 1904069 (2019).

[11] J. Li, C. Shen, X. Zhu, Y. Xie, and S. A. Cummer, Nonreciprocal sound propagation in space-time modulated media, Phys. Rev. B **99**, 144311 (2019).

[12] J. Marconi, E. Riva, M. Di Ronco, G. Cazzulani, F. Braghin, and M. Ruzzene, Experimental Observation of Nonreciprocal Band Gaps in a Space-Time-Modulated Beam Using a Shunted Piezoelectric Array, Phys. Rev. Appl. **13**, 031001(R) (2020).

[13] A. E. Cardin, S. R. Silva, S. R. Vardeny, W. J. Padilla, A. Saxena, A. J. Taylor, W. J. Kort-Kamp, H.-T. Chen, D. A. Dalvit, and A. K. Azad, Surface-wave-assisted nonreciprocity in spatio-temporally modulated metasurfaces, Nat. Commun. **11**, 1469 (2020).

[14] H. Ammari, J. Cao, and E. O. Hiltunen, Nonreciprocal wave propagation in space-time modulated media, Multiscale Model. Simul. **20**, 1228 (2022).

[15] Z. Wu and A. Grbic, Serrodyne frequency translation using time-modulated metasurfaces, IEEE Trans. Antennas Propag. **68**, 1599 (2019).

[16] S. Taravati and G. V. Eleftheriades, Full-Duplex Nonreciprocal Beam Steering by Time-Modulated Phase-Gradient Metasurfaces, Phys. Rev. Appl. **14**, 014027 (2020).

[17] L. Zhang, M. Z. Chen, W. Tang, J. Y. Dai, L. Miao, X. Y. Zhou, S. Jin, Q. Cheng, and T. J. Cui, A wireless communication scheme based on space-and frequency-division multiplexing using digital metasurfaces, Nat. Electron **4**, 218 (2021).

[18] X. Wang, V. S. Asadchy, S. Fan, and S. Tretyakov, Space-time metasurfaces for perfect power combining of waves, ACS Photonics **8**, 3034 (2021).

[19] Y. Chen, X. Li, H. Nassar, A. N. Norris, C. Daraio, and G. Huang, Nonreciprocal Wave Propagation in a Continuum-Based Metamaterial with Space-Time Modulated Resonators, Phys. Rev. Appl. **11**, 064052 (2019).

[20] G. Castaldi, L. Zhang, M. Moccia, A. Y. Hathaway, W. X. Tang, T. J. Cui, and V. Galdi, Joint multi-frequency beam shaping and steering via space–time-coding digital metasurfaces, Adv. Funct. Mater. **31**, 2007620 (2021).

[21] P. A. Huidobro, E. Galiffi, S. Guenneau, R. V. Craster, and J. B. Pendry, Fresnel drag in space–time-modulated metamaterials, Proc. Natl. Acad. Sci. USA **116**, 24943 (2019).

[22] J. C. Serra and M. G. Silveirinha, Rotating spacetime modulation: Topological phases and spacetime haldane model, Phys. Rev. B **107**, 035133 (2023).

[23] X. Wen, X. Zhu, H. W. Wu, and J. Li, Realizing spatiotemporal effective media for acoustic metamaterials, Phys. Rev. B **104**, L060304 (2021).

[24] I. V. Lindell and A. H. Sihvola, Perfect electromagnetic conductor, J. Electromagn. Waves. Appl. **19**, 861 (2005).

[25] I. V. Lindell and A. H. Sihvola, Transformation method for problems involving perfect electromagnetic conductor (PEMC) structures, IEEE Trans. Antennas Propag. **53**, 3005 (2005).

[26] A. Maurel, J.-J. Marigo, K. Pham, and S. Guenneau, Conversion of Love waves in a forest of trees, Phys. Rev. B **98**, 134311 (2018).

[27] A. Alu, G. D'Aguanno, N. Mattiucci, and M. J. Bloemer, Plasmonic Brewster Angle: Broadband Extraordinary Transmission through Optical Gratings, Phys. Rev. Lett. **106**, 123902 (2011).

[28] A. N. Norris and X. Su, Enhanced acoustic transmission through a slanted grating, C. R. Mécanique **343**, 622 (2015).

[29] R. Porter, Plate arrays as a perfectly-transmitting negative-refraction metamaterial, Wave Motion **100**, 102673 (2021).

[30] H. T. To, *Homogenization of Dynamic Materials* (Temple University Press, Philadelphia, 2004).

[31] H. T. To, Homogenization of dynamic laminates, J. Math. Anal. Appl. **354**, 518 (2009).

[32] M. Kreiczer and Y. Hadad, Wave Analysis and Homogenization of a Spatiotemporally Modulated Wire Medium, Phys. Rev. Appl. **16**, 054003 (2021).
[33] P. A. Huidobro, M. G. Silveirinha, E. Galiffi, and J. B. Pendry, Homogenization Theory of Space-Time Metamaterials, Phys. Rev. Appl. **16**, 014044 (2021).
[34] F. R. Prudêncio and M. G. Silveirinha, Synthetic axion response with spacetime crystals, arXiv:2209.03314.
[35] K. Pham and A. Maurel, Diffraction grating with space-time modulation, J. Comput. Phys. **469**, 111528 (2022).
[36] J.-J. Marigo and A. Maurel, Second order homogenization of subwavelength stratified media including finite size effect, SIAM J. Appl. Math. **77**, 721 (2017).
[37] A. Ourir and M. Fink, Active control of the spoof plasmon propagation in time varying and non-reciprocal metamaterial, Sci. Rep. **9**, 2368 (2019).
[38] J. Zhou Hagström, A. Maurel, and K. Pham, The interplay between Fano and Fabry–Pérot resonances in dual-period metagratings, Proc. R. Soc. A. **477**, 20210632 (2021).
[39] P. Roux and M. Fink, Experimental evidence in acoustics of the violation of time-reversal invariance induced by vorticity, Europhys. Lett. **32**, 25 (1995).
[40] L. Kelders, J. Allard, and W. Lauriks, Ultrasonic surface waves above rectangular-groove gratings, J. Acoust. Soc. Am. **103**, 2730 (1998).
[41] J. Pendry, L. Martin-Moreno, and F. Garcia-Vidal, Mimicking surface plasmons with structured surfaces, Science **305**, 847 (2004).
[42] J.-F. Mercier, M.-L. Cordero, S. Félix, A. Ourir, and A. Maurel, Classical homogenization to analyse the dispersion relations of spoof plasmons with geometrical and compositional effects, Proc. R. Soc. A: Math. Phys. Eng. Sci. **471**, 20150472 (2015).
[43] X.-R. Huang, R.-W. Peng, and R.-H. Fan, Making Metals Transparent for White Light by Spoof Surface Plasmons, Phys. Rev. Lett. **105**, 243901 (2010).
[44] A. Maurel, S. Félix, and J.-F. Mercier, Enhanced transmission through gratings: Structural and geometrical effects, Phys. Rev. B **88**, 115416 (2013).
[45] A. Maurel and J.-J. Marigo, Sensitivity of a dielectric layered structure on a scale below the periodicity: A fully local homogenized model, Phys. Rev. B **98**, 024306 (2018).
[46] K. Pham, A. Maurel, J.-F. Mercier, S. Félix, M. L. Cordero, and C. Horvath, Sensitivity of a dielectric layered structure on a scale below the periodicity: A fully local homogenized model, Wave Motion **93**, 102485 (2020).
[47] A. Castanié, J.-F. Mercier, S. Félix, and A. Maurel, Generalized method for retrieving effective parameters of anisotropic metamaterials, Opt. Express **22**, 29937 (2014).
[48] A. Maurel, K. Pham, and J.-J. Marigo, Homogenization of thin 3d periodic structures in the time domain–effective boundary and jump conditions, Fund. Applicat. Acous. Metamater. **1**, 73 (2019).
[49] S. Tretyakov, A. Sihvola, A. Sochava, and C. Simovski, Magnetoelectric interactions in bi-anisotropic media, J. Electromagn. Waves. Appl. **12**, 481 (1998).
[50] C. Tai, A study of electrodynamics of moving media, Proc. IEEE **52**, 685 (1964).